

Titre: Numerical predictions in turbomachinery analysis
Title:

Auteurs: Marcelo Reggio, Ricardo Camarero, & Thi C. Vu
Authors:

Date: 1985

Type: Rapport / Report

Référence: Reggio, M., Camarero, R., & Vu, T. C. (1985). Numerical predictions in turbomachinery analysis. (Rapport technique n° EPM-RT-85-07).
Citation: <https://publications.polymtl.ca/10048/>

 **Document en libre accès dans PolyPublie**
Open Access document in PolyPublie

URL de PolyPublie: <https://publications.polymtl.ca/10048/>
PolyPublie URL:

Version: Version officielle de l'éditeur / Published version

Conditions d'utilisation: Tous droits réservés / All rights reserved
Terms of Use:

 **Document publié chez l'éditeur officiel**
Document issued by the official publisher

Institution: École Polytechnique de Montréal

Numéro de rapport: EPM-RT-85-07
Report number:

URL officiel:
Official URL:

Mention légale:
Legal notice:



EPM/RT-85-7

380-62-38⁽²⁾

207

(NUMERICAL PREDICTIONS IN TURBOMACHINERY ANALYSIS)

Don
Marcelo (Reggio), Ricardo (Camarero)* and (Thi) C. Vu **

* Ecole Polytechnique de Montréal

** Dominion Engineering Works, Montréal

Ecole Polytechnique de Montréal

Février 1985

This work was carried out with the financial support of the PRAI project #P-8122, from the NSERC of Canada and the Ministère de la Science et Technologie du Québec, in collaboration with D.E.W.

Tous droits réservés. On ne peut reproduire ni diffuser aucune partie du présent ouvrage, sous quelque forme que ce soit, sans avoir obtenu au préalable l'autorisation écrite de l'auteur.

Dépot légal , 2^e trimestre 1985
Bibliothèque nationale du Québec
Bibliothèque nationale du Canada

Pour se procurer une copie de ce document, s'adresser au:

Service de l'édition
Ecole Polytechnique de Montréal
Case Postale 6079, Succ. "A"
Montréal, Québec H3C 3A7
(514) 340-4903

Compter 0,05\$ par page (arrondir au dollar le plus près), plus 1,50\$ (Canada) ou 2,50\$ (étranger) pour la couverture, les frais de poste et la manutention. Régler en dollars canadiens par chèque ou mandat-poste au nom de l'Ecole Polytechnique de Montréal. Nous n'honorons que les commandes accompagnées d'un paiement, sauf s'il y a eu entente préalable, dans le cas d'établissements d'enseignement ou d'organismes canadiens.

1. INTRODUCTION

Progress of the design process in turbomachinery demands a maximization of the power recovery while at the same time a minimization of the energy losses. The ability to respond to this kind of requirements is related to the availability of appropriate analysis tools. In this context the prediction of the physics inside a blade passage is crucial.

The objective of this report is to present a numerical procedure to solve time-dependent incompressible Navier-Stokes equations through a cascade of blades. The proposed method is based on the primitive-variable formulation using a control volume approach. The main difficulties associated with the solution of this type of problem are: the treatment of the boundary conditions on the geometries that bounds the domain, the choice of a proper storage location for the dependent variables and the lack of an explicit equation for the pressure.

In the present effort the problem of the complex boundaries is treated by formulating and solving the conservation equations on a curvilinear coordinate system that matches the boundary domain. This procedure is straightforward and universal, because the boundary nodes always coincide with the domain boundary, and no particular procedure is required at these locations.

Among the techniques that can be used to numerically create a curvilinear mesh, the body-fitted method has been adopted. Such system

proposed by Thompson[1] and incorporated on a software package devised by Garon[2] is used for the mesh generation.

An effective cell structure to deal with incompressible fluid flows is the staggered grid[3] formulation. This technique avoids a checkerboard pattern for velocity and pressure fields, but increases the complexity by requiring a different location together with a different computational cell for each velocity component and the pressure. In the development presented here, only one computational cell is needed, and velocity components and pressure are computed at the same location. Furthermore the good qualities of the staggered mesh formulation are preserved by using an opposed difference scheme for pressure and fluxes.

A pressure equation for a curvilinear system was derived on the basis of the SIMPLE[4] method and applied to obtain a satisfactory pressure field that meets the mass constraint requirement.

2. GOVERNING EQUATIONS

When solving the equations of motion on a curvilinear coordinate system, it seems natural to use as dependent variables velocity the components along these coordinates. In doing so the scalar equations (as continuity and energy) are in conservation law form, but not the momentum equation (a vectorial one) due to source like terms appearing as Christoffel Symbols[5]. These terms correct the momentum components of a fluid that is "constrained" to move along

a path defined by a coordinate which is not a straight line[6]. However as every mesh point belongs to a different vector basis, if the change in angle and vector basis length from grid point to grid point is severe, despite the correction, the numerical calculation could suffer.

A way to solve this problem is to keep the cartesian velocity components as the dependent variables. In this case all properties will be in the conservation law form (momentum is conserved on a straight line). The resulting system is hybrid where both cartesian and contravariant components coexist, but these equations are not significantly more complex than their cartesian counterpart, and the discrete approximations can be easily handled.

Following this approach, the time dependent Navier-Stokes equations can be written in strong conservative form as[7]:

$$\frac{\partial q}{\partial t} + \frac{\partial E}{\partial \xi} + \frac{\partial F}{\partial \eta} = \frac{\partial R}{\partial \xi} + \frac{\partial S}{\partial \eta} \quad (1)$$

where:

$$q = J \begin{bmatrix} 0 \\ u \\ v \end{bmatrix} \quad E = J \begin{bmatrix} U \\ uU + p\xi_x \\ vU + p\xi_y \end{bmatrix} \quad F = J \begin{bmatrix} V \\ uV + p\eta_x \\ vV + p\eta_y \end{bmatrix}$$

$$R = \mu J \begin{bmatrix} g^{11}u_\xi + g^{12}u_\eta \\ g^{11}v_\xi + g^{12}v_\eta \end{bmatrix} \quad S = \mu J \begin{bmatrix} g^{21}u_\xi + g^{22}u_\eta \\ g^{21}v_\xi + g^{22}v_\eta \end{bmatrix}$$

and μ represents the viscosity.

The contravariant velocity components U, V along the curvilinear coordinates and the cartesian velocity components u, v are related by:

$$U = u\xi_x + v\xi_y$$

(2)

$$V = u\eta_x + v\eta_y$$

The metric terms $\xi_x, \xi_y, \eta_x, \eta_y$, the jacobian J and the contravariant metric tensor components g^{11}, g^{12}, g^{21} , and g^{22} are obtained from:

$$\xi_x = y_\eta/J, \quad \xi_y = -x_\eta/J$$

$$\eta_x = -y_\xi/J, \quad \eta_y = x_\xi/J$$

$$J = x_\xi y_\eta - x_\eta y_\xi$$

$$g^{11} = \xi_x^2 + \xi_y^2$$

$$g^{12} = \xi_x \eta_x + \xi_y \eta_y$$

$$g^{21} = g^{12}$$

$$g^{22} = \eta_x^2 + \eta_y^2$$

3. GRID LAYOUT

The most frequent grid structure used in the numerical solution of incompressible fluid flow problems was initially introduced for cartesian geometries by Harlow and Welch [3], and is known as the staggered grid. In this arrangement the pressure is stored at the center of the cell, while the different velocity components are stored at the vertical and horizontal faces respectively. Although this disposition has demonstrated the ability to avoid a checkerboard pattern for velocity and pressure fields its implementation for a curvilinear system where more than a velocity component has to be stored on each face lead to some difficulties. As a result of this, in the present work it is proposed a different scheme and grid arrangement that preserves the good properties of the staggered mesh, while alleviating the geometric complications and computer implementation generally encountered when using curvilinear coordinates.

The proposed structure stores pressure and cartesian velocity components at the center $(i+1/2, j)$ of a computational element made up of one width in the "streamwise" coordinate direction and two units in the other. The grid cell is shown on fig.1. This computational cell is used for both mass and momentum calculations. It has to be noted that while the momentum equations involve the curvilinear and cartesian velocity components, the mass conservation depends only on the contravariant velocity components U and V , located at the center of the faces $i, i+1$ and

$j-1, j+1$ of the element shown on fig. (1) respectively.

4. DISCRETIZATION

Based on the above grid pattern, the equations are discretized to obtain a system of algebraic equations.

Second order differences are used to evaluate mass and pressure gradients in the η direction. The velocity values at the $j+1$ and $j-1$ faces (fig.1) are calculated by overlapping elements in that direction; while the pressure is obtained by a simple average of two neighbours points in the same direction.

In the ξ direction no overlapping or averaging is used, this time the treatment is done in a different manner. Mass gradients are obtained by upwind differencing, so the flux through the downwind face $i+1$ is controlled by the velocity at the center $i+1/2, j$ of the element. Pressure gradients on the other hand, are calculated via downwind differences, that is to say, that the pressure located at the cell center $i + 1/2, j$ acts on the upstream face i .

A similar treatment for the solution of the compressible Euler equations can be found in [8], and an interesting analysis of the opposed difference idea, is given in [9]. Recently Fuchs and Zhao[10] have also presented a combination of forward and backward differences coupled with the multigrid method. References [9] and [10] solve the steady viscous equations.

The scheme is explicit and in compact form can be written as:

$$\Delta q + \Delta t (E_{\epsilon} + F_{\eta})^n = \Delta t (R_{\epsilon} + S_{\eta})^n \quad (3)$$

where Δ denotes the forward time difference operator and n the time level.

4a) Continuity Equation

From this form, and from the definition of equation (1) the discrete approximation of the continuity equation with the superscript n dropped is written as:

$$\frac{(JU)_{i+1,j} - (JU)_{i,j}}{\Delta \xi} + \frac{(JV)_{i+1/2,j+1} - (JV)_{i+1/2,j-1}}{2\Delta \eta} = 0 \quad (4)$$

This equation involves the contravariant velocities U and V at the cell faces (that is not the case of the cartesian components located at the cell center), and it is noted that only one component is required to calculate the mass flow through each face. For a better understanding of the way that these components are computed, some details concerning the scheme and variables storage are given.

The cartesian velocity components are calculated and stored at the center $(i+1/2, j)$ of the computational cell with corners $(i, j-1; i+1, j-1; i+1, j+1; i, j+1)$ (fig.1). However due to the overlapping in the j direction these properties are also known at the center of the face $i+1/2, j+1$, because they correspond to values the values of the cell center with corners $(i, j; i+1, j; i+1, j+2; i, j+2)$ (fig.2). The same reasoning applies for the $j-1$ level.

With the known cartesian velocities at all j levels (due to the overlapping grid), the V components at $j \pm 1$ faces are obtained from (2) as:

$$V_{i+1/2, j \pm 1} = U_{i+1/2, j \pm 1} (\eta_x)_{i+1/2, j \pm 1} + V_{i+1/2, j \pm 1} (\eta_y)_{i+1/2, j \pm 1} \quad (5)$$

As mentioned earlier, the cartesian velocity components obtained from the momentum equations are computed at the center $i+1/2, j$ of the computational cell, and are not known at the required locations

i,j and $i+1,j$. To calculate the required U components at such levels upwinding is used for the mass flow; and they are obtained from equation (2) as:

$$U_{i,j} = u_{i-1/2,j} (E_x)_{i,j} + v_{i-1/2,j} (E_y)_{i,j} \quad (6)$$

$$U_{i+1,j} = u_{i+1/2,j} (E_x)_{i+1,j} + v_{i+1/2,j} (E_y)_{i+1,j}$$

4b) Momentum Equations

The discrete form of the momentum equations requires the knowledge of the convected momentum fluxes and diffusion terms at the cell faces. These terms are evaluated by adopting the weighted upstream difference scheme of Raithby and Torrance[11]; for example the convected property u and the diffusion term $g^{11} du/d\xi$ at the upstream face are calculated by:

$$u_{i,j} = (1/2 + \alpha_{i,j}) u_{i-1/2} + (1/2 - \alpha_{i,j}) u_{i+1/2,j} \quad (7)$$

and

$$C_{i,j} = g^{11} du/d\xi|_{i,j} = g^{11} \beta_{i,j} \frac{(u_{i+1/2,j} - u_{i-1/2})}{\Delta \xi} \quad (8)$$

where α and β are coefficients depending on the Peclet number[12].

With these terms known the momentum equation written for example for the u component becomes:

$$\begin{aligned}
 & J_{i+1/2,j} \frac{(u^{n+1} - u^n)_{i+1/2,j}}{\Delta t} \\
 & + \frac{(JuU)_{i+1,j} - (JuU)_{i,j}}{\Delta \xi} \\
 & + \frac{(JuV)_{i+1/2,j+1} - (JuV)_{i+1/2,j-1}}{2\Delta \eta} \\
 & + \frac{p_{i+3/2,j} (J\xi_x)_{i+1,j} - p_{i+1/2,j} (J\xi_x)_{i,j}}{\Delta \xi} \\
 & + \frac{p_{i+1/2,j+1} (J\eta_x)_{i+1/2,j+1} - p_{i+1/2,j-1} (J\eta_x)_{i+1/2,j-1}}{2\Delta \eta} \\
 & + \frac{C_{i,j} - C_{i+1,j}}{\Delta \xi} + \frac{C_{i+1/2,j+1} - C_{i+1/2,j-1}}{2\Delta \eta} = 0 \quad (9)
 \end{aligned}$$

5. SOLUTION PROCEDURE

The algorithm starts by guessed pressure and velocity fields, from which the cartesian momentum equations are solved. Denoted by u^* and v^* the resulting velocity components that do not conserve mass, are then substituted into equations (5) and (6) to compute the contravariant velocity components U^* and V^* .

The next step, and probably the most difficult when solving incompressible flow problems is to correct the U^* and V^* velocities in such a manner to yield a pressure field which drives velocities that satisfy mass conservation.

The approach followed to handle the velocity-pressure coupling

problem is based on the principle of the SIMPLE[4] method. According to this technique the momentum equations are used to obtain relations between corrections to the velocity and pressure fields which violate the continuity condition.

The momentum equations are written twice, once for velocity and pressure fields that do not verify the continuity constraint, and then for fields that satisfy mass conservation.

For example the discretized x momentum equation is written for a u^* and p^* 's that violate mass conservation as:

$$u^*_{i+1/2,j} = u^*_{i+1/2,j} + \Delta t \left\{ \frac{p^*_{i+1/2,j} (J\xi_x)_{i,j} - p^*_{i+3/2,j} (J\xi_x)_{i+1,j}}{J_{i+1/2,j} \Delta\xi} \right. \\ \left. - \frac{p^*_{i+1/2,j+1} (J\eta_x)_{i+1/2,j+1} - p^*_{i+1/2,j-1} (J\eta_x)_{i+1/2,j-1}}{2\Delta\eta} \right. \\ \left. - \text{FLUX} + \text{VISC} \right\} \quad (10)$$

where FLUX and VISC represents the resulting convected and viscous terms over the element respectively.

In the same manner the equation for a velocity u and a pressure $p = p^* + \delta p$ that meets the mass constraint requirement is written as:

$$\begin{aligned}
 u_{i+1/2,j} = u_{i+1/2,j} + \Delta t \left\{ \frac{p_{i+1/2,j} (J\xi_x)_{i,j} - p_{i+3/2,j} (J\xi_x)_{i+1,j}}{J_{i+1/2,j} \Delta\xi} \right. \\
 \left. + \frac{p_{i+1/2,j+1} (J\eta_x)_{i+1/2,j+1} - p_{i+1/2,j-1} (J\eta_x)_{i+1/2,j-1}}{2\Delta\eta} \right\} \\
 \text{-FLUX +VISC} \qquad (11)
 \end{aligned}$$

subtracting (10) from (11) one obtains:

$$\begin{aligned}
 \delta u = (u - u^*)_{i+1/2,j} = \Delta t \left\{ \frac{\delta p_{i+1/2,j} (J\xi_x)_{i,j} - \delta p_{i+3/2,j} (J\xi_x)_{i+1,j}}{J_{i+1/2,j} \Delta\xi} \right. \\
 \left. + \frac{\delta p_{i+1/2,j+1} (J\eta_x)_{i+1/2,j+1} - \delta p_{i+1/2,j-1} (J\eta_x)_{i+1/2,j-1}}{2\Delta\eta} \right\} \\
 (12)
 \end{aligned}$$

Following the same procedure a similar equation for the v component can be found.

With this cartesian velocity corrections $\delta u = u - u^*$ and $\delta v = v - v^*$ known, the corresponding expressions for the curvilinear velocity corrections $\delta V = U - U^*$ and $\delta V = V - V^*$ are found by using analogous expressions to relations (2), that is:

$$\delta U = \delta u \xi_x + \delta v \xi_y \quad (13)$$

$$\delta V = \delta u \eta_x + \delta v \eta_y$$

Equations (13) depends on the pressure corrections δp , so a relation to obtain these correction is needed. This is achieved by using the continuity equation written in terms of velocity components U, V and U^*, V^* that do and do not satisfy mass conservation respectively, the discrete form of the latter is written as:

$$\frac{(JU^*)_{i+1,j} - (JU^*)_{i,j}}{\Delta \xi} + \frac{(JV^*)_{i+1/2,j+1} - (JV^*)_{i+1/2,j-1}}{2\Delta \eta} = D \quad (14)$$

where D depends represents a mass source term. Substraction of (14) from (4) gives:

$$\frac{(J\delta U^*)_{i+1,j} - (J\delta U^*)_{i,j}}{\Delta \xi} + \frac{(J\delta V^*)_{i+1/2,j+1} - (J\delta V^*)_{i+1/2,j-1}}{2\Delta \eta} = -D \quad (15)$$

This equation involves 9 pressure points, however if only the pressure correction at the center $i+1/2, j$ of the element is retained, while the effect of the neighbouring pressures is neglected

one obtains a definitive equation for the pressure change

$$\delta p_{i+1/2,j} = f^p(\delta U, \delta V, D)$$

In the present approach the pressure adjustment is done cell by cell as in the MAC method[13].

Once δp is evaluated at the cell center, the curvilinear velocity corrections δU and δV are calculated, then all corrections combined with the inexact velocity and pressure fields in order to verify the mass constraint; that is:

$$\begin{aligned} U &= U^* + \delta U \\ V &= V^* + \delta V \\ p &= p^* + \delta p \end{aligned} \tag{16}$$

To modify the variables over the entire computational domain the grid is swept point-by-point in the inlet-outlet direction. Improved values are immediately used as the procedure advances. This procedure is repeated until all cells have D values less than a desired level of accuracy.

When the above step is completed, only one curvilinear

velocity component that meets the mass constraint requirement is known on each face (U and V on the η and ξ faces respectively). To obtain the "missing" component averaging of surrounding velocities that satisfy continuity is used [12]. Then the cartesian velocity components are decoded as the boundary conditions applied.

Finally the time level is advanced and the cycle repeated until the steady state is reached.

6. APPLICATIONS

6.1 Cascade Analysis

In order to analyse the predictions features of the present model, a first application to turbomachinery was carried out by computing the flow on a NACA [14] cascade. The discretisation employed 90×27 grid points and several tests up to $Re=20,000$ were conducted and for an angle of attack of 30° .

The computational grid for this case is given in fig.3 where the blade-to-blade passage is shown to illustrate the grid distribution.

Figure 4. illustrates the velocity field obtained for $Re=2000$, while fig.5 shows the calculated S coefficient (defined as $S = 1 - C_p$) compared with the experimental values (Ref.14) The over all agreement is good, in particular the peak pressure at the leading edge is

well captured together with a good simulation of the diffusion flow on the suction side. However the trailing edge prediction shows some discrepancy.

A comparison of the computed aerodynamics parameters, such as lift and drag coefficients, outlet angle and losses, has been carried out with the experimental data of Ref [14] and the results are presented on table 1. It can be appreciated that the outlet angle and the lift coefficient are reasonably well predicted for all Reynolds numbers, however the drag coefficient is much higher than the experimental value. This can be attributed to the intrinsic numerical viscosity arising from the discretization process; a similar phenomenon was also found in a finite element solution on the same geometry [15].

A second cascade test was done on a blade passage reported by Langston et al. [16]. The experimental data presented by these authors is for a three-dimensional experience, however due to the constant cross section it is reasonable to attempt a comparison with the data reported at the midspan of the channel.

Figure 6 shows the calculated (using 48x19 mesh points and for $Re=1000$) and experimental static pressure coefficient on the blade surface. The pressure side shows a good agreement of values and the overall trend is well predicted. On the suction side the pressure distribution presents some quantitative disagreement near the minimum. This can be attributed to the absence of the secondary flow movement perceived in the three-dimensional

flow[17];in spite of that the trailing edge pressure distribution is well predicted

Table 2. shows the calculated aerodynamic parameters for $Re=1000$ and $Re=5000$, and the available experimental data.As in the previous case and for the same reason,the numerical value of the aerodynamic loss is greater than the experimental,in spite of that,the computed outlet angle conforms very well the measured value given in [16].

After these basic verifications completed a more complex application to turbomachinery was attempted by studying the flow through two blade passages one after the other.This kind of configuration found on the spiral casing of the hydraulics turbines is formed by the stay vane and the wicket gate.The first passage is static while the second is of variable angle.A general view of the forementioned geometry is given in fig.7.

A representative illustration of the passage form is shown on fig.8, and a typical body-fitted mesh used to predict the flow on this sort of problem is depicted on fig.9.

The flow through these two cascades in series was fully tested for different angles of attack of the wicket gate and for different Reynolds numbers,this latter defined in terms of the throat radius.

Figure 10 presents the velocity field obtained on a characteristic channel.For this example the Reynolds number is of 10,000, the stay vane angle is of 34.5° ,the wicket angle of $33.^\circ$,and

the inlet and outlet flow angles of 20° and 37.96° respectively.

This general representation allows to visualize particular regions of interest, such as the zone nearby the trailing edge of the stay vane and the leading edge of the wicket gate, where the flow undergoes rapid changes.

The skin friction coefficient calculated on the surfaces of the blades is displayed as function of the normalized cord (Fig.11) The full line is used to indicate the wicket gate and the dotted for the stay vane, arrows represent the suction side. This kind of information is quite useful in the design process; in particular it is noted that when the skin friction coefficient becomes negative reverse flow and separation occurs.

In the same way that in the previous diagram, fig.12 represents the S coefficient as function of the cord. Because the purpose of the forementioned blades is not to produce lift but to induce the flow, the knowledge of this variable is useful to minimize the area between the pressure and suction side curves.

As mentioned earlier several tests for different attack angles of the wicket gate were conducted in the diffuser passage. The information obtained from these tests was then used to build a plot where isocontours of energy losses are displayed as function of wicket gate opening and attack angle. This information is illustrated on fig.13 from which it can be appreciated for example, that for the first ten degrees of variation of the attack angle (from 20° to 30°),

the energy losses change is considerable; while that for the last ten degrees (between 50° and 60°) this variation is minimal.

A further study was done by performing a quasi-3d analysis on a Kaplan turbine. On fig.14 a representation on the Z-R plane of the mesh and the potential flow path, including the intake, runner and draft tube is presented. Figure 15 shows a partial view of the set of blades (for sake of clarity only some of them are drawn) where the numbers are to indicate the sections that are developed to work out 2-D investigations.

Figures 16 and 17 illustrate the resulting developed blade profile on sections 2 and 5. Computations were done for these and for the remaining sections (3 and 4) using 90x27 grid points for $Re=10,000$ and where different angles of attack are imposed on each blade-to-blade portion. The obtained velocity fields for the levels of figs. 16 and 17 are drawn on figs. 18 and 19. The corresponding calculated pressure coefficient is depicted as a function of the nondimensional cord on figs. 20 and 21.

A comparison of the results obtained from the quasi-3D analysis with the available experimental data has been done and is illustrated on fig. 22. In this picture the tangential velocity components for the different levels are drawn as function of the radius and the nondimensional speed ratio ξ ($\xi = u_{abs}/\sqrt{2gH}$, where u_{abs} represents the absolute tangential velocity, g the gravity constant and H the head). The concordance of numerical and experimental values is very good for the inner sections, however some disparity is observed for the

outer levels.

A procedure to solve incompressible flows on arbitrary shapes without using a staggered formulation has been developed. This is accomplished by the use of an opposed-difference scheme. Applications to compute the flow through cascades have been done. The reported results are satisfactory and show that the proposed method is a plausible tool for turbomachinery analysis.

REFERENCES:

1. R.Camarero and M.Younis , Efficient Generation of Body-Fitted Coordinates for Cascades using Multigrid , AIAA Journal vol 18, pp. 487-488 ,1980
2. A. Garon, and R. Camarero, Interactive Turbomachinery Design, NUMETA 85, International Conference Series on Advances in Numerical Methods in Engineering: Theory and Applications, University College, Swansea, January 7-11 ,1985
3. F.H Harlow and J.E. Welch, Numerical Calculation of Time Dependent Viscous Incompressible Flow of Fluid with Free Surface, Phys.Fluids, Vol. 8, no 12, pp 2182-2189,1965
4. S.V. Patankar, Numerical Heat Transfer and Fluid Flow Hemisphere, Washington., 1980
5. P.R Eisman and P. Stone, Conservation Laws of Fluids Dynamics -A Survey, SIAM Review, vol 22 pp.12-27,1980
6. D. Schnack and J. Killeen, Nonlinear, Two-Dimensional Magnetohydrodynamic Calculations, Journal of Computational Physics, vol.35, pp110-145, 1980

7. R. Peyret and H. Viviand, Computation of Viscous Compressible Flow Based on the Navier-Stokes Equation, North Atlantic Treaty Organization, AGARD 212 , 1975
8. J.D Denton, A Time Marching Method for Two and Three Dimensional Blade-to-Blade Flows, A.R.C., REM 3775 ,1975
9. D.F Roscoe, The Numerical Solution of the Navier-Stokes Equations for Three-Dimensional Laminar Flow in Curved Pipes using Finite Differences Methods, J. of Engineering Mathematics, vol 12, pp 303-323,1978
10. Fuchs, L. and Zhao H-S., Solution of Three-Dimensional Viscous Incompressible Flow By A Multigrid Method, Int. Journal for Numerical Methods in Fluids, vol. 4 ,pp 539-555, 1984
11. G.D Raitby and K.E Torrance, Upstream Weighted Differencing Schemes and their Application to Elliptic Problems Involving Fluid Flows, Computer Fluids vol. 2, pp 191-206, 1974
12. C.R Maliska, A Solution Method for Three-Dimensional Parabolic Fluid Flow Problems in Nonorthogonal Coordinates", Ph. D. Thesis, University of Waterloo, Canada, 1981
13. C.W Hirt, B.D Nichols and N.C Romero, SOLA- A Numerical Solution Algorithm for Transient Fluid Flows, 1975, Los Alamos Scientific Laboratory, Report LA-5852, 1975

14. J.C. Dunavant and J.R Erwin, Investigation of a Related Series of a Turbine-Blade Profiles in a Cascade, NACA T.R. Note 3802, 1956

15. A. Fortin ,R. Camarero , T. C. Vu, and M. Fortin, Simulation Numérique d'Écoulements Visqueux dans une Turbine Hydraulique,Rapport Technique, Ecole Polytechnique de Montréal,1985

16. L.S. Langston, M.L. Nice and R.M Hooper, Three-Dimensional Flow Within a Turbine Cascade Passage, ASME Journal of Engineering for Power ,vol.99 no. 1 pp.21-28, 1977

17. C. Hah, A Navier-Stokes Analysis of Three-Dimensional Turbulent Flows Inside Turbine Blade Rows at Desing and Off-Desing Conditions, ASME Paper 83-GT-40

TABLE 1

Comparison of experimental (Ref. 14) and computed values

	Re= 50	Re= 1000	Re=20,000	Experimental
C_D	1.33	0.38	0.23	0.04
C_L	1.46	1.41	1.36	1.6
Losses	125%	42%	28%	---
outlet angle	43.2	41.3	38	42.6

TABLE 2

Comparison of experimental (Ref. 16) and computed values

	Re= 1,000	Re= 5,000	Experimental
C_D	2.03	1.70	---
C_L	2.74	2.72	---
Losses	135%	135%	25%
outlet angle	64.4	63.5	64

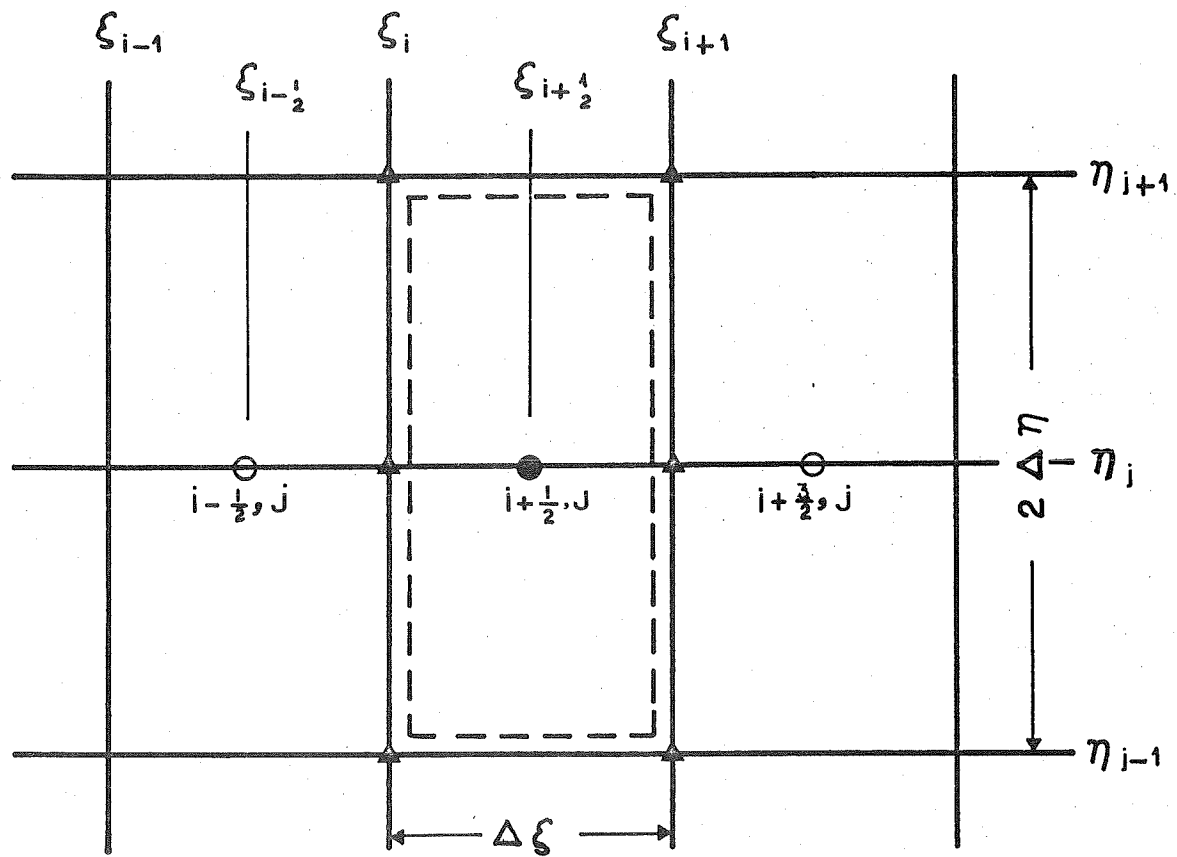


Fig. 1 Basic Computational Cell

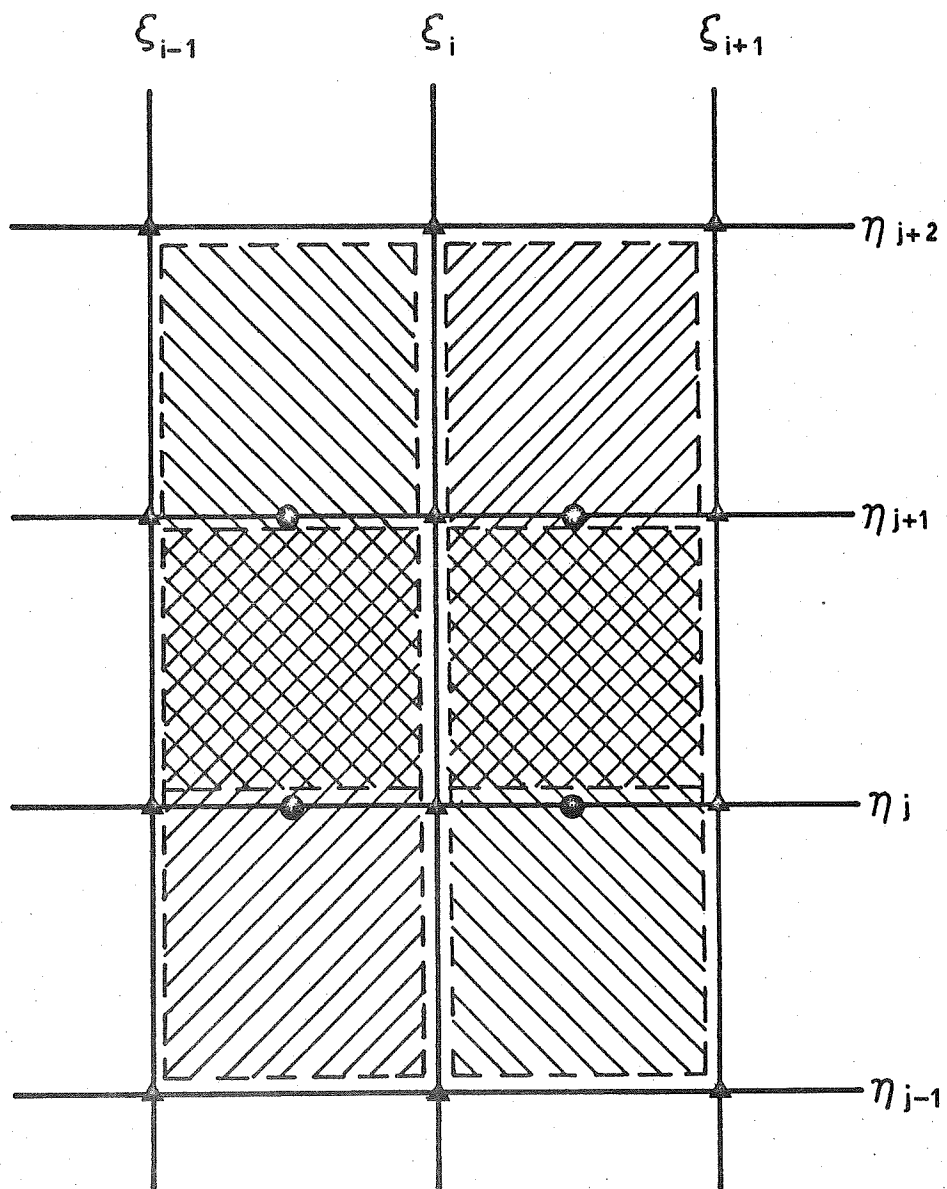


Fig. 2 Overlapping Grid

CARACTERISTIQUES DU PROFIL

PROFIL = C50.PRO
CORDE = 1.000
NOMBRE DE PTS = 30

CARACTERISTIQUES DE LA CASCADE

NOMBRE DE RANGEES = 27
NO. TOTAL COLONNE = 90
NO. COL. ENTREE = 30
NO. COL. SORTIE = 30

LONG. INTERAUBE = 0.6666
LONG. ENTREE = 1.000
LONG. SORTIE = 1.000

ANGLE ENTREE (DEC) = 30.00
ANGLE PROFIL (DEC) = -25.00
ANGLE SORTIE (DEC) = -40.00

CONC. RANGEES = 0.6000
CONC. COL. ENTREE = 0.3000
CONC. COL. SORTIE = 0.3000

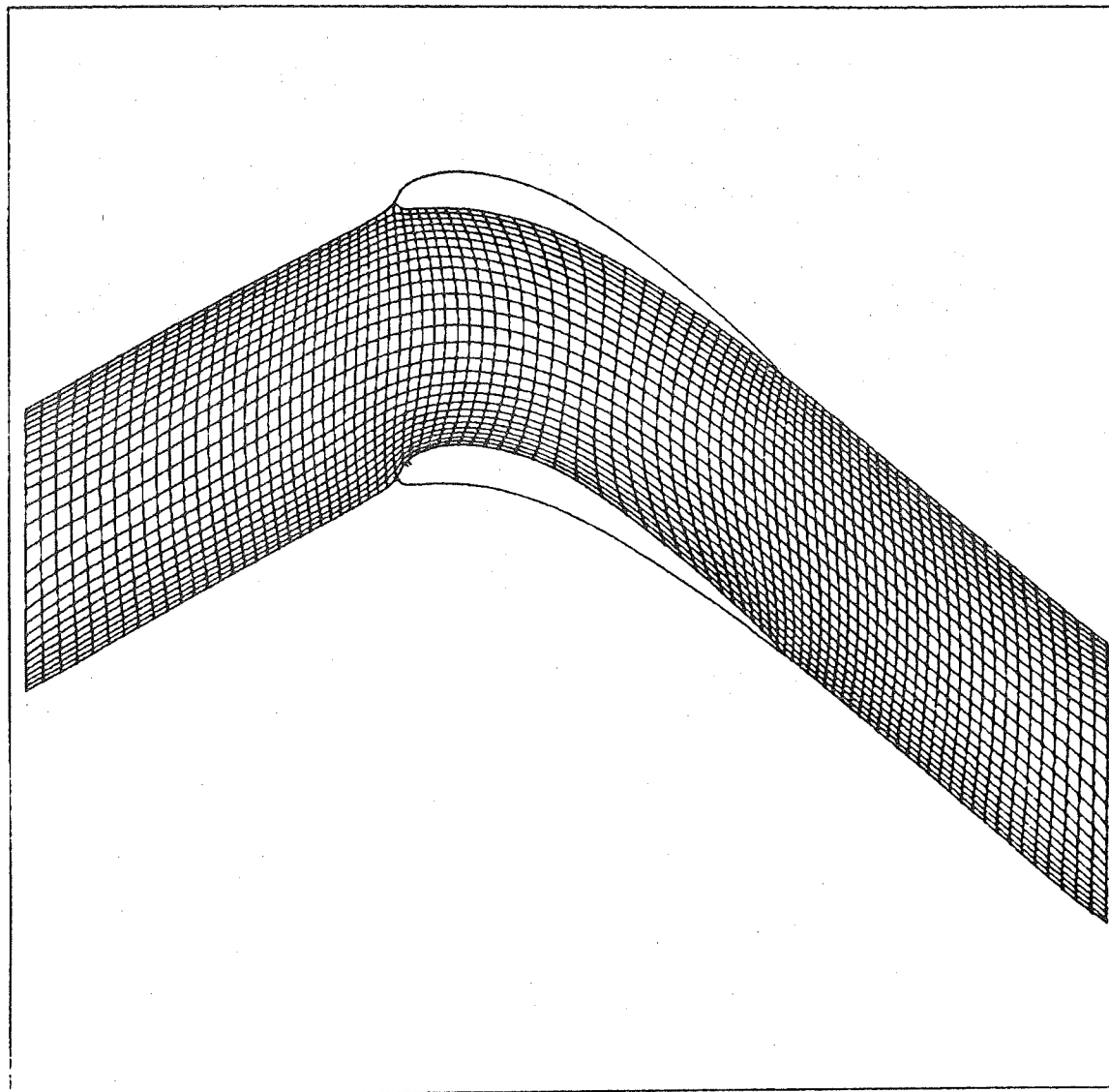


Fig. 3 Body-Fitted Grid for the Cascade of Ref. (14)

ANALYSE DIF - NACA00

SOLUTION R2000.056

ECOULEMENT VISQUEUX
REYNOLDS = 2000.0

ANGLE PROFIL = -25.00
ANGLE ATTAQUE = 30.00
ANGLE FUI TE = -30.98

COEF. CD = 0.3160
COEF. CL = 1.397
COEF. CA = 0.4371
COEF. CT = 1.364
TOPOUE CM = -1.385

CARACTERISTIQUES DU PROFIL

PROFIL = C50.PRO
CORDE = 1.000
NOMBRE DE PTS = 30

CARACTERISTIQUES DE LA CASCADE

CASCADE = 056 CAS
NOMBRE DE RANGEE = 27
NO. TOTAL COLONNE = 86
NO. COL. ENTREE = 28
NO. COL. SORTIE = 28

LONG. INTERAUBE = 0.6650
LONG. ENTREE = 1.000
LONG. SORTIE = 1.000

ANGLE ENTREE (DEG) = 30.00
ANGLE PROFIL (DEG) = -25.00
ANGLE SORTIE (DEG) = -40.00

CONC. RANGEES = 0.6000
CONC. COL. ENTREE = 0.3000
CONC. COL. SORTIE = 0.3000

COMPOSANT UX MAX = 1.456
(RANG= 6 ,COL.=33)
COMPOSANT UX MIN = -0.1132E-01
(RANG= 2 ,COL.=57)

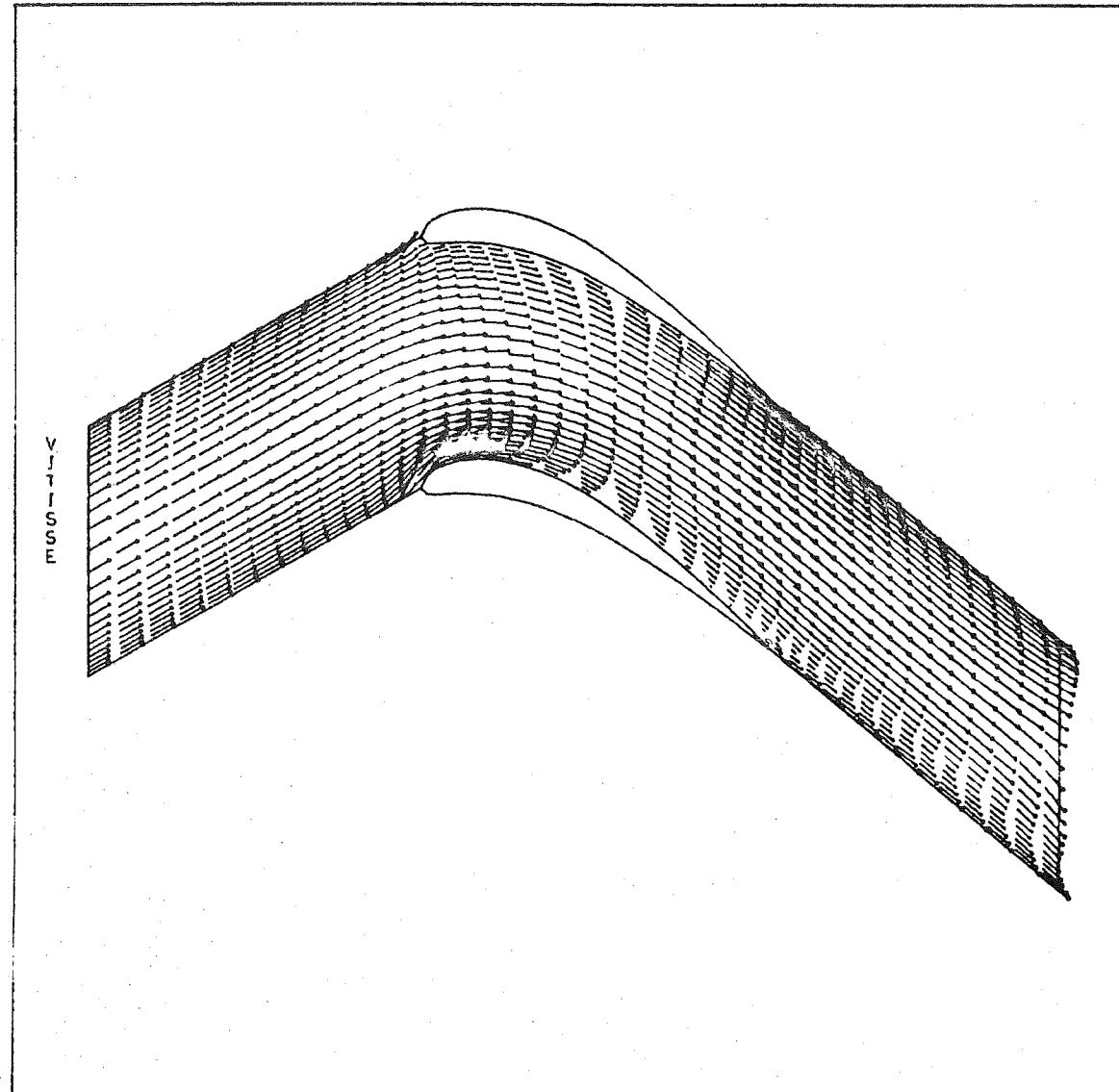


Fig. 4 Velocity field for Re = 2000

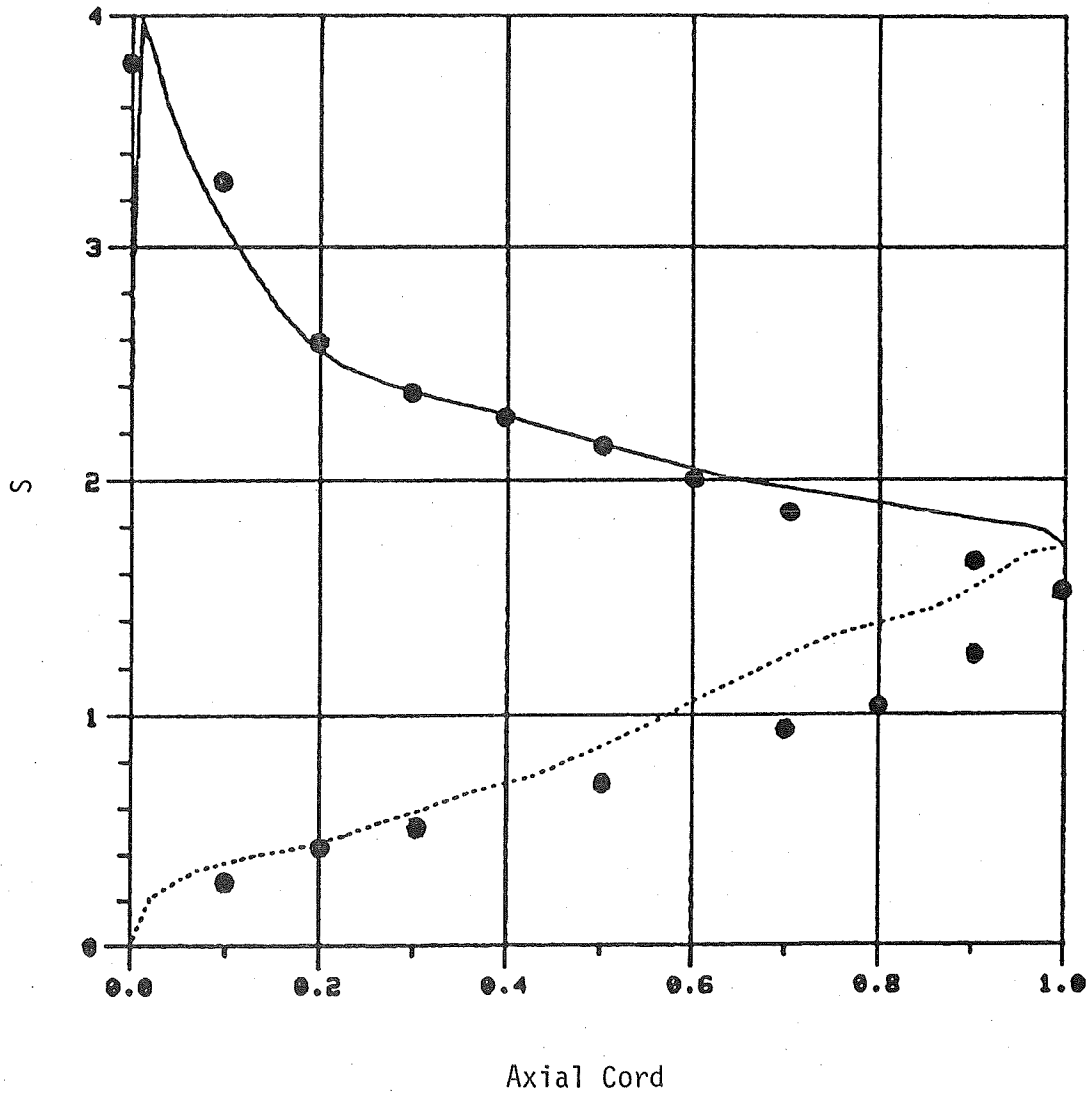


Fig. 5 Calculated and Experimental (represented by dots) coefficient for the profile of Ref. 14

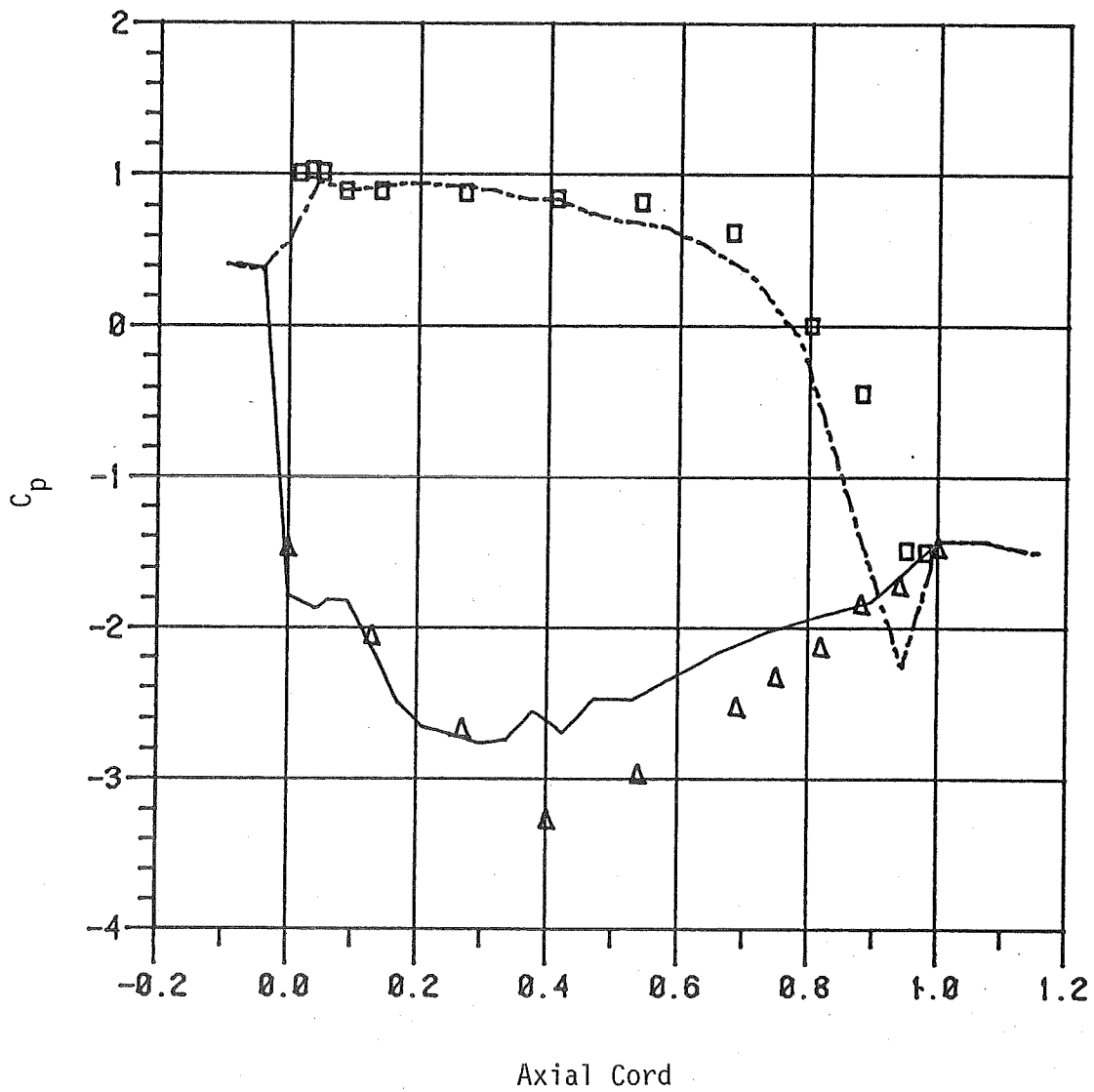


Fig. 6 Calculated and Experimental (represented by triangles and squares) pressure coefficient for the profile of Ref. 16

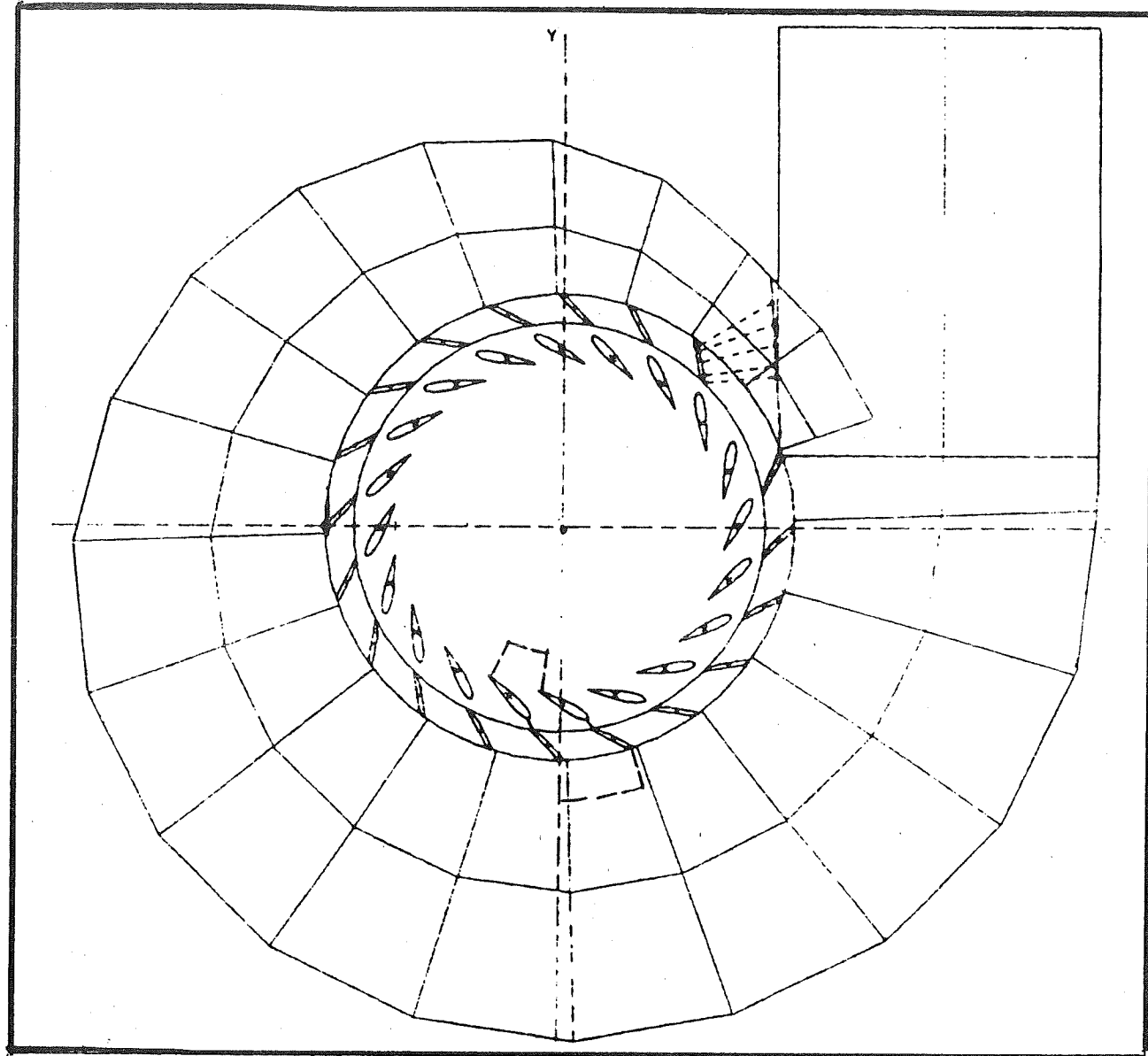


Fig. 7 SPIRAL CASING PLAN VIEW

CARACTERISTIQUES DE LA CASCADE

CASCADE	=	A3533.CAS	
NOMBRE DE RANGEE	=	27	
NO.TOTAL COLONNE	=	141	
RAYON DE GORGE	=	79.00	(1.00)
ANGLE PERIODIQUE	=	18.00	(DEG)
LOC.RAD. DU PIVOT	=	88.00	(1.11)
LOC.ANG. DU PIVOT	=	7.25	(DEG)
(P/R BORD FUIITE 1)			
PROFIL1	=	STU.PRO	
LOC.RAD.BORD ATTAQ	=	121.8	(1.54)
LOC.RAD.BORD FUIITE	=	104.3	(1.32)
CORDE	=	27.22	(0.34)
ANGLE PROFIL 1	=	34.50	(DEG)
NOMBRE DE PTS	=	35	
PROFIL2	=	UKG.PRO	
LOC.RAD.BORD ATTAQ	=	101.0	(1.28)
LOC.RAD.BORD FUIITE	=	80.85	(1.02)
CORDE	=	33.06	(0.42)
ANGLE PROFIL 2	=	33.00	(DEG)
NOMBRE DE PTS	=	41	
LONG. ENTREE	=	25.00	(0.32)
ANGLE ENTREE	=	35.00	(DEG)
LONG. SORTIE	=	35.00	(0.44)
ANGLE SORTIE	=	45.00	(DEG)
NO. COL. ENTREE	=	25	
NO. COL. INTER	=	5	
NO. COL. SORTIE	=	35	
SONC. RANGEES	=	0.60	
SONC. COL. ENTREE	=	0.30	
SONC. COL. INTER	=	0.10	
SONC. COL. SORTIE	=	0.30	

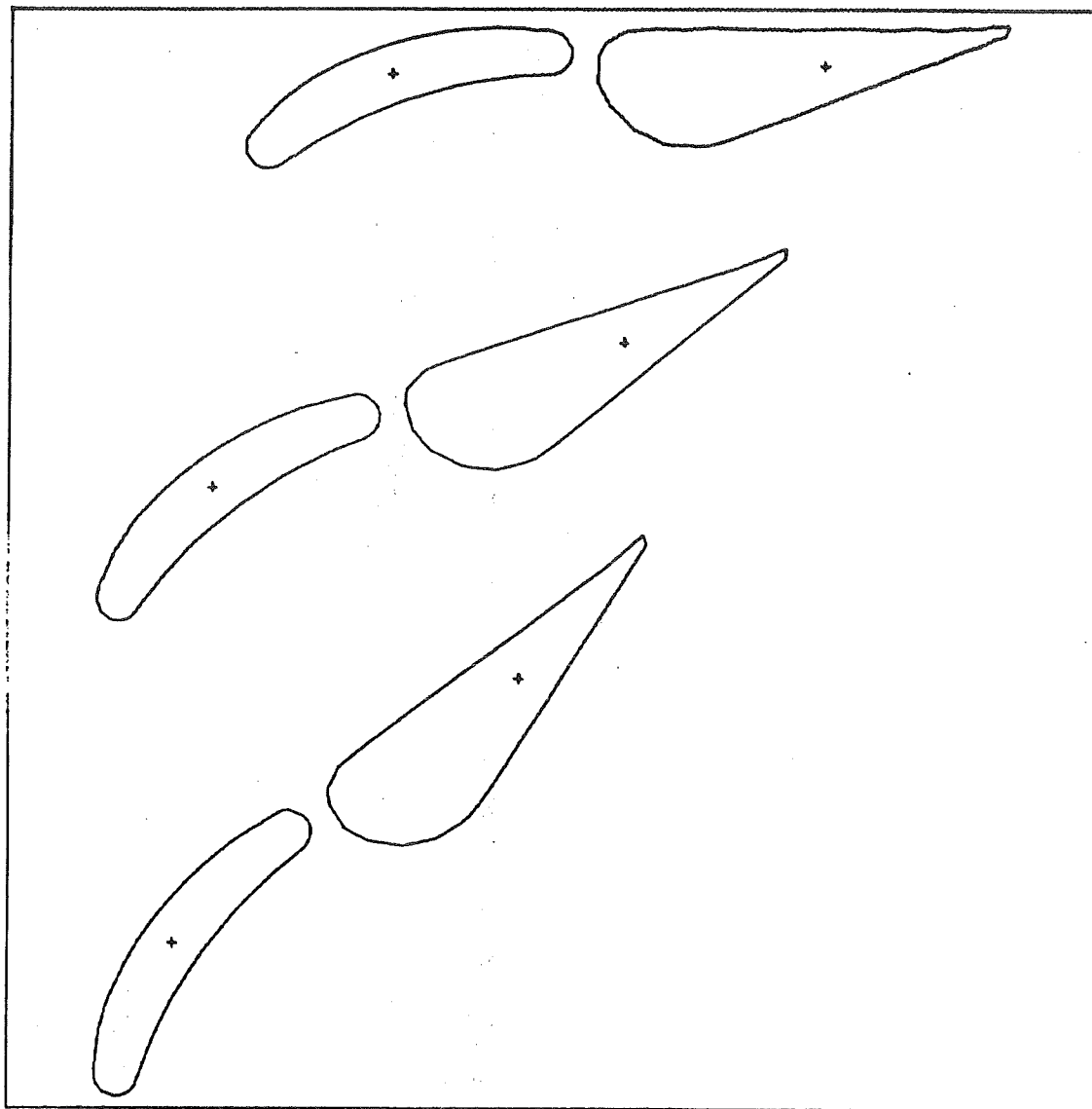


Fig. 8 Consecutive Cascades

CHARACTERISTIQUES DE LA CASCADE

CASCADE	•	A3533.CAS	
NOMBRE DE RANGEES	•	27	
NO. TOTAL COLONNE	•	141	
RAYON DE GORGE	•	79.00	(1.00)
ANGLE PERIODIQUE	•	18.00	(DEG)
LOC. RAD. DU PIVOT	•	88.00	(1.11)
LOC. ANG. DU PIVOT	•	7.25	(DEG)
(P/R BORD FUIITE 1)			
PROFIL1	•	STU.PRO	
LOC. RAD. BORD ATTAQ	•	121.8	(1.54)
LOC. RAD. BORD FUIITE	•	104.3	(1.32)
CORDE	•	27.22	(0.34)
ANGLE PROFIL 1	•	34.50	(DEG)
NOMBRE DE PTS	•	35	
PROFIL2	•	WKG.PRO	
LOC. RAD. BORD ATTAQ	•	101.0	(1.28)
LOC. RAD. BORD FUIITE	•	80.85	(1.02)
CORDE	•	33.06	(0.42)
ANGLE PROFIL 2	•	33.00	(DEG)
NOMBRE DE PTS	•	41	
LONG. ENTREE	•	25.00	(0.32)
ANGLE ENTREE	•	35.00	(DEG)
LONG. SORTIE	•	35.00	(0.44)
ANGLE SORTIE	•	45.00	(DEG)
NO. COL. ENTREE	•	25	
NO. COL. INTER	•	5	
NO. COL. SORTIE	•	35	
CONC. RANGEES	•	0.60	
CONC. COL. ENTREE	•	0.30	
CONC. COL. INTER	•	0.10	
CONC. COL. SORTIE	•	0.30	

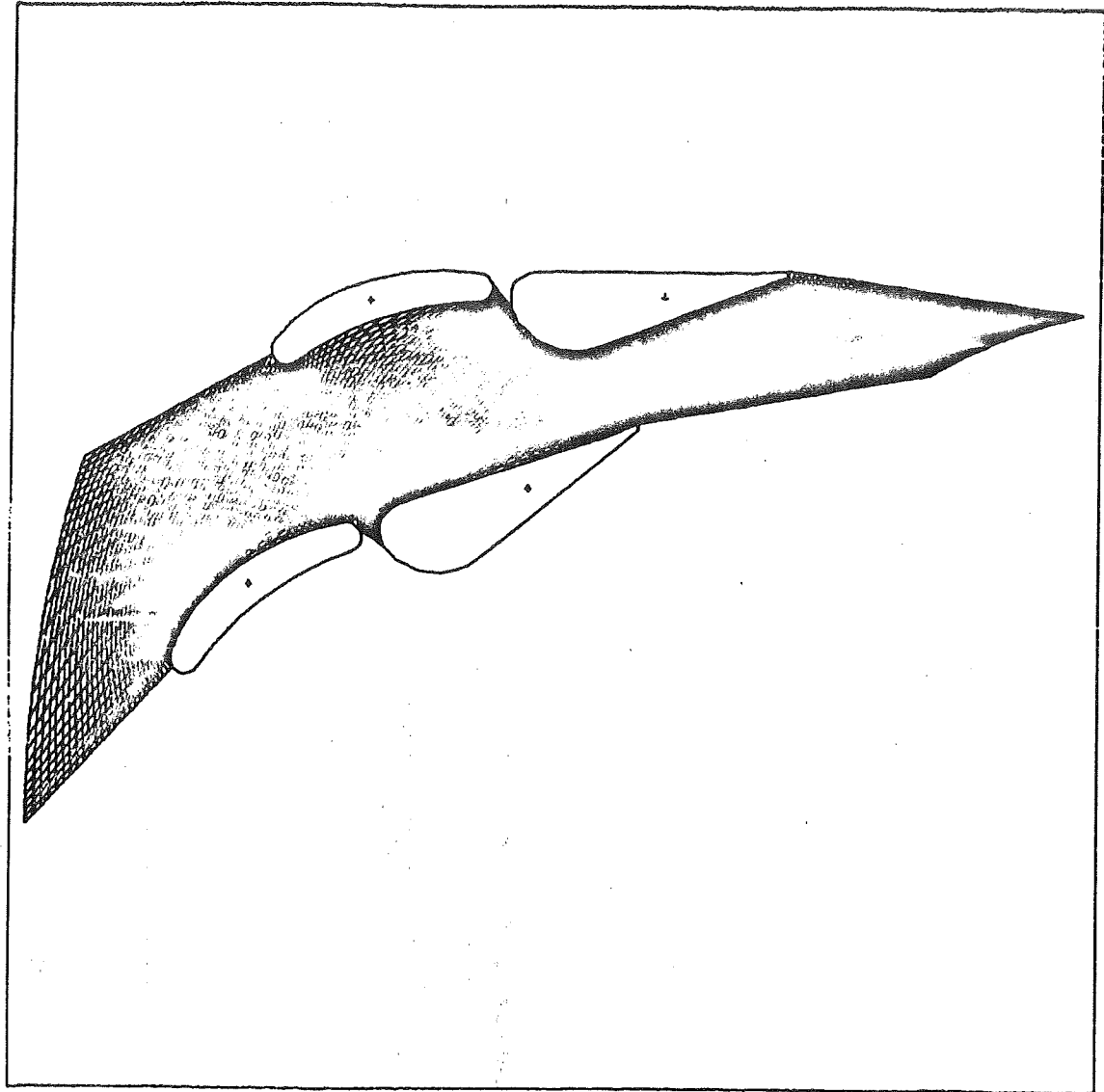


Fig. 9 Body-Fitted Mesh for Two Consecutive Cascades

ISLE MALIGNE - SYM.WGT

OLUTION F3533.A30

COULEMENT VISQUEUX
EYNOLDS = 10000.

NGLE ATTAQUE = 30.00
NGLE FUITE = 27.82

ARACTERISTIQUES DE LA CASCADE

ASCADÉ = F3533.CAS
OMBRE DE RANGEE = 27
O.TOTAL COLONNE = 143

AYON DE GORGE = 79.00 (1.00)
NGLE PERIODIQUE = 18.00 (DEG)

OC.RAD. DU PIVOT = 88.00 (1.11)
OC.ANG. DU PIVOT = 7.25 (DEG)
P/R BORD FUITE 1)

ROFIL1 = STU.PRO
OC.RAD.BORD ATTAQ = 121.8 (1.54)
OC.RAD.BORD FUITE = 104.3 (1.32)
ORDE = 27.22 (0.34)
NGLE PROFIL 1 = 34.50 (DEG)
OMBRE DE PTS = 35

ROFIL2 = UKGLPR.PRO
OC.RAD.BORD ATTAQ = 96.70 (1.22)
OC.RAD.BORD FUITE = 81.05 (1.03)
ORDE = 28.88 (0.37)
NGLE PROFIL 2 = 33.00 (DEG)
OMBRE DE PTS = 41

ONG. ENTREE = 25.00 (0.32)
NGLE ENTREE = 35.00 (DEG)

ONG. SORTIE = 40.00 (0.51)
NGLE SORTIE = 45.00 (DEG)

O. COL. ENTREE = 25
O. COL. INTER = 7
O. COL. SORTIE = 35

ONG. RANGEES = 0.60
ONG. COL. ENTREE = 0.30
ONG. COL. INTER = 0.10
ONG. COL. SORTIE = 0.30

OMPOSANT UX MAX = 3.397
RANG = 2 , COL. = 142)
OMPOSANT UX MIN = -0.4660
RANG = 3 , COL. = 60)

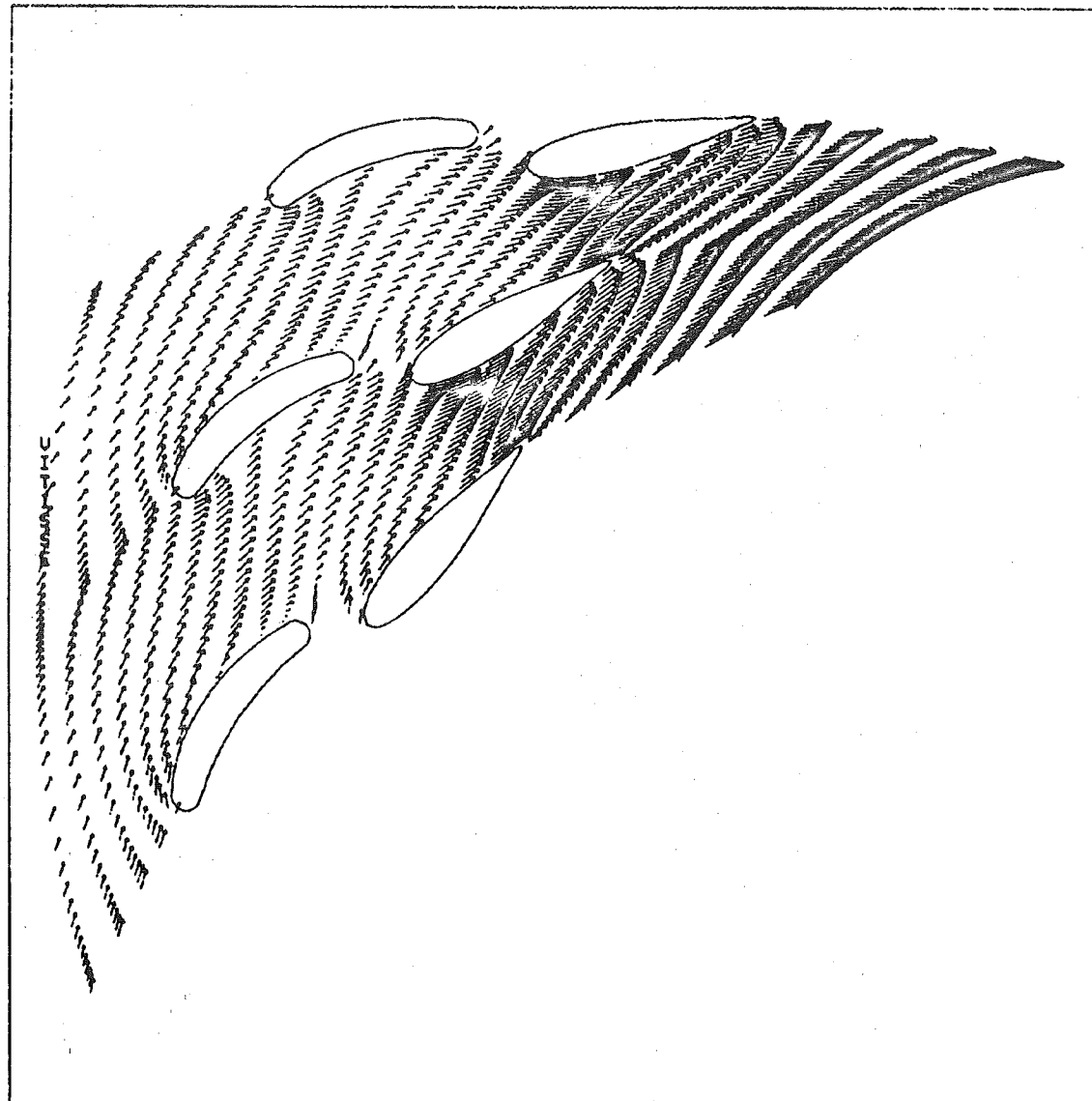


Fig. 10 Velocity Field for Two Successive Cascades

ISLE MALIGNE - SYM.UGT

OLUTION F3533.A30

COULEMENT VISQUEUX
EYNOLDS = 10000.

NGLE ATTAQUE = 30.00
 NGLE FUITE = 27.82
 OEF. CD = 0.3911
 OEF. CL = 0.4984E-01
 ORQUE CM = 0.1421
 OEF. CD = -0.1049
 OEF. CL = -3.611
 ORQUE CM = 0.2519

ARACTERISTIQUES DE LA CASCADE

ASCADÉ = F3533.CAS
 NOMBRE DE RANGEES = 27
 O.TOTAL COLONNE = 143

AYON DE GORGE = 79.00 (1.00)
 NGLE PERIODIQUE = 18.00 (DEG)

OC.RAD. DU PIVOT = 88.00 (1.11)
 OC.ANG. DU PIVOT = 7.25 (DEG)
 P/R BORD FUITE 1)

ROFIL1 = STU.PRO
 OC.RAD.BORD ATTAQ = 121.8 (1.54)
 OC.RAD.BORD FUITE = 104.3 (1.32)
 ORDE = 27.22 (0.34)
 NGLE PROFIL 1 = 34.50 (DEG)
 NOMBRE DE PTS = 35

ROFIL2 = UKGLPR.PRO
 OC.RAD.BORD ATTAQ = 96.70 (1.22)
 OC.RAD.BORD FUITE = 81.05 (1.03)
 ORDE = 28.88 (0.37)
 NGLE PROFIL 2 = 33.00 (DEG)
 NOMBRE DE PTS = 41

ONG. ENTREE = 25.00 (0.32)
 NGLE ENTREE = 35.00 (DEG)

ONG. SORTIE = 40.00 (0.51)
 NGLE SORTIE = 45.00 (DEG)

O. COL. ENTREE = 25
 O. COL. INTER = 7
 O. COL. SORTIE = 35

ONC. RANGEES = 0.60
 ONC. COL. ENTREE = 0.30
 ONC. COL. INTER = 0.10
 ONC. COL. SORTIE = 0.30

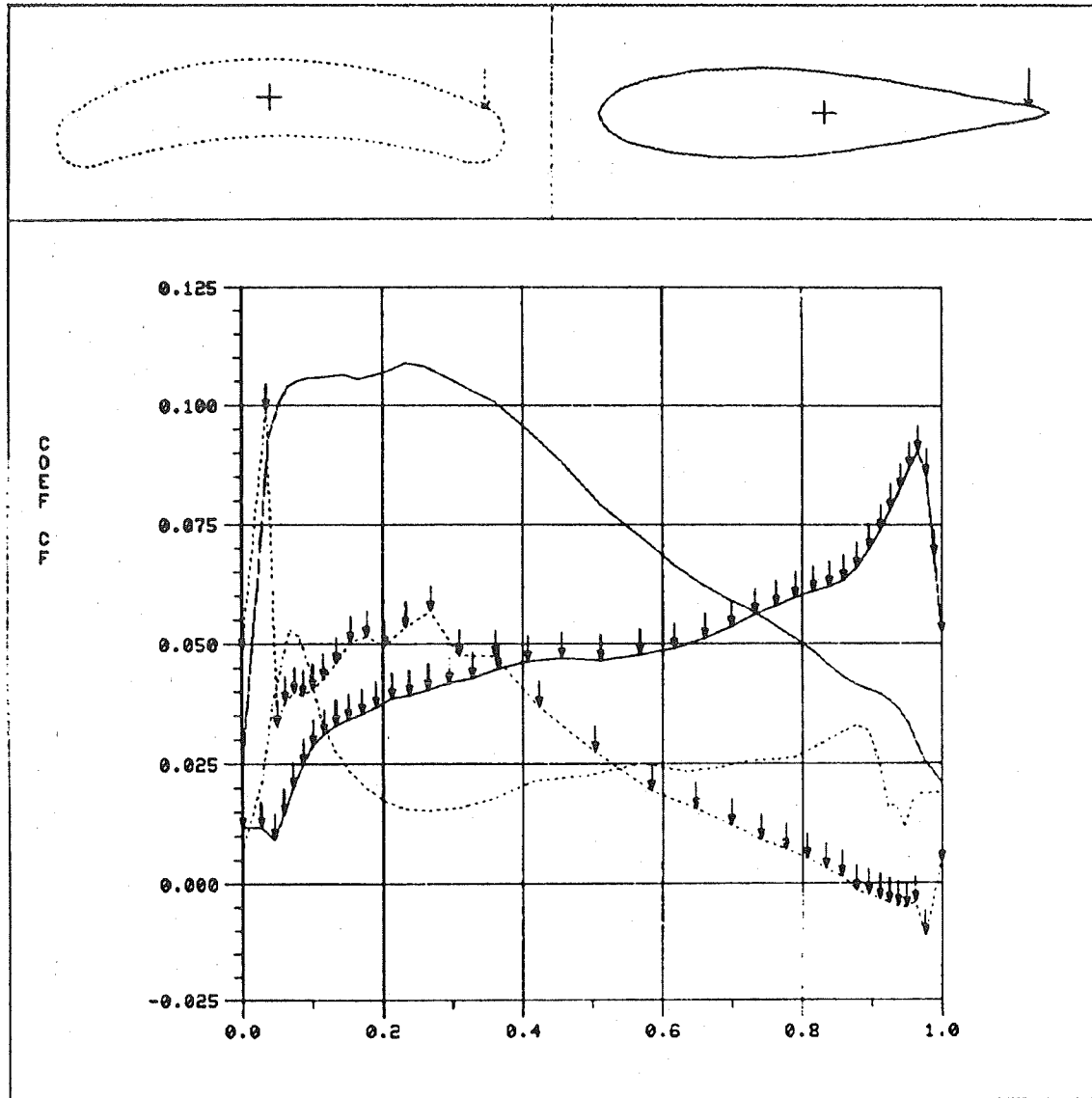


Fig. 11 Skin Friction Coefficient as
Function of the Normalized Length

ISLE MALIGNE - SYM.UGT

OLUTION F3533.A30

COULEMENT VISQUEUX
REYNOLDS = 10000.

ANGLE ATTAQUE = 30.00
ANGLE FUIITE = 27.82

ARACTERISTIQUES DE LA CASCADE

CASCADE = F3533.CAS
OMBRE DE RANGEE = 27
O.TOTAL COLONNE = 143

AYON DE GORGE = 79.00 (1.00)
NGLE PERIODIQUE = 18.00 (DEG)

.OC.RAD. DU PIVOT = 88.00 (1.11)
.OC.ANG. DU PIVOT = 7.25 (DEG)
P/R BORD FUIITE 1)

ROFIL1 = STU.PRO
.OC.RAD.BORD ATTAQ = 121.8 (1.54)
.OC.RAD.BORD FUIITE = 104.3 (1.32)
ORDE = 27.22 (0.34)
NGLE PROFIL 1 = 34.50 (DEG)
OMBRE DE PTS = 35

ROFIL2 = UKGLPR.PRO
.OC.RAD.BORD ATTAQ = 96.70 (1.22)
.OC.RAD.BORD FUIITE = 81.05 (1.03)
ORDE = 28.88 (0.37)
NGLE PROFIL 2 = 33.00 (DEG)
OMBRE DE PTS = 41

.ONG. ENTREE = 25.00 (0.32)
NGLE ENTREE = 35.00 (DEG)

.ONG. SORTIE = 40.00 (0.51)
NGLE SORTIE = 45.00 (DEG)

O. COL. ENTREE = 25
O. COL. INTER = 7
O. COL. SORTIE = 35

ONG. RANGEES = 0.60
ONG. COL. ENTREE = 0.30
ONG. COL. INTER = 0.10
ONG. COL. SORTIE = 0.30

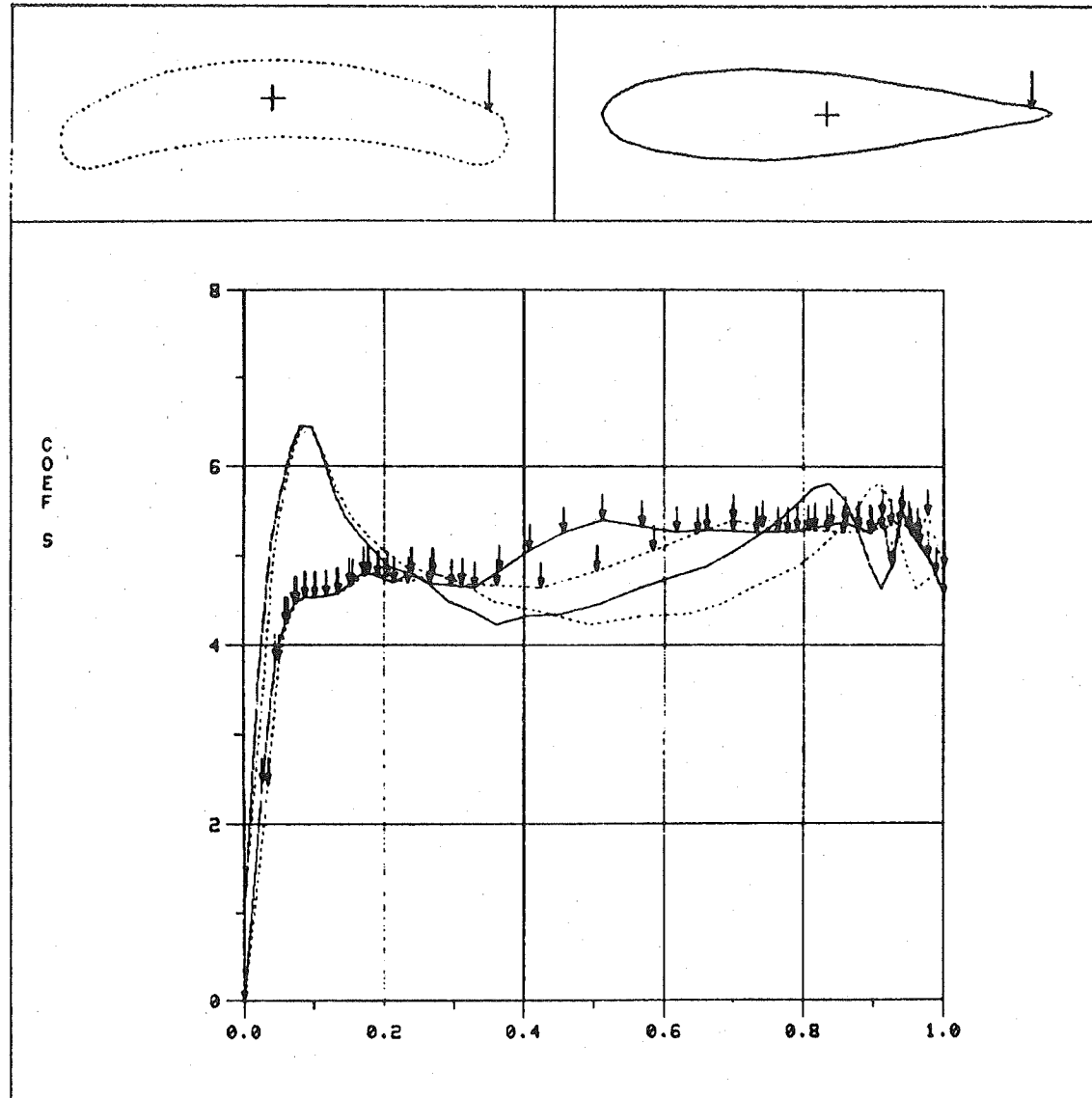


Fig. 12 S Coefficient as Function of the Normalized Length

MENU PRINCIPAL :

- > Lecture de données sur (TER)minaal
- > Lecture de données sur (FIC)hier
- > Tracage des courbes de (COM)tour
- > Tracage des courbes de (PER)formance
- > (E)CRIre les données sur fichier
- > (FIN)
- .. : Abreviation
- > Entrer une option :

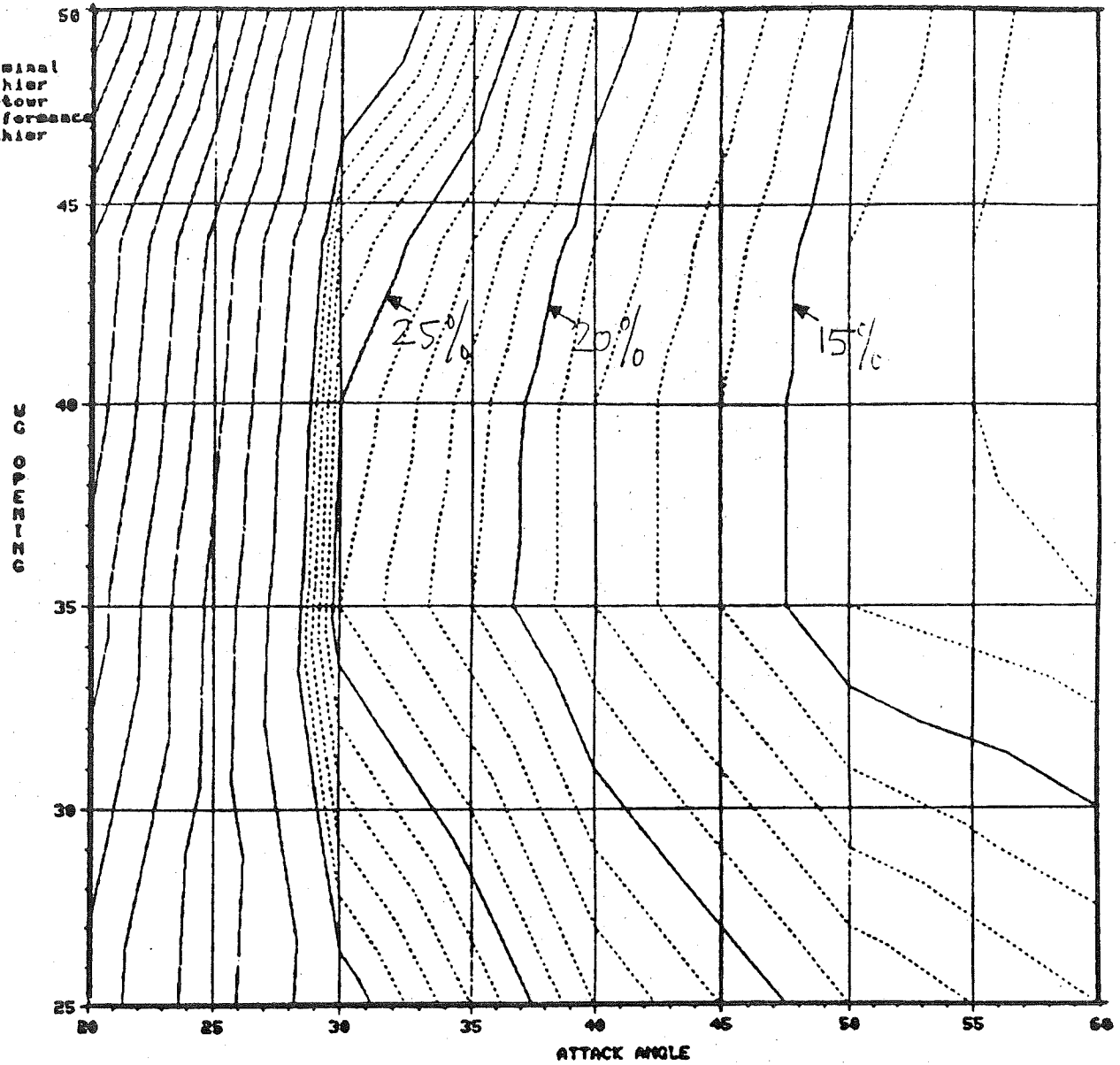


Fig. 13 Isocontours of Energy Losses

K-349 A=3.0
THROUGHFLOW
SURFACE 1

PAUSE FOR COPY

17-JAN-85 11:25:11

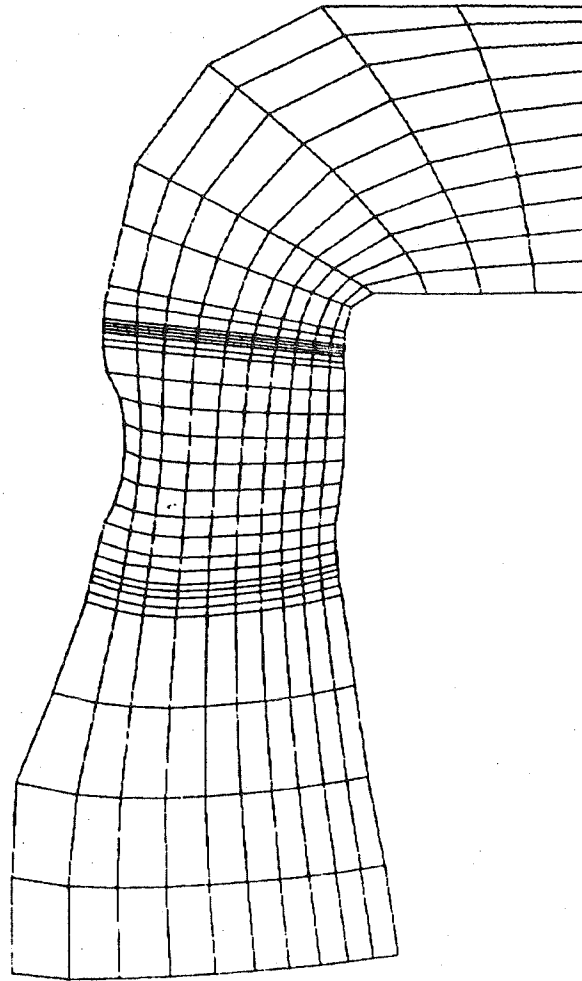


Fig. 14 Throughflow Grid for a Kaplan
Runner on the Z-R Plane

A-342 PHI=1.45

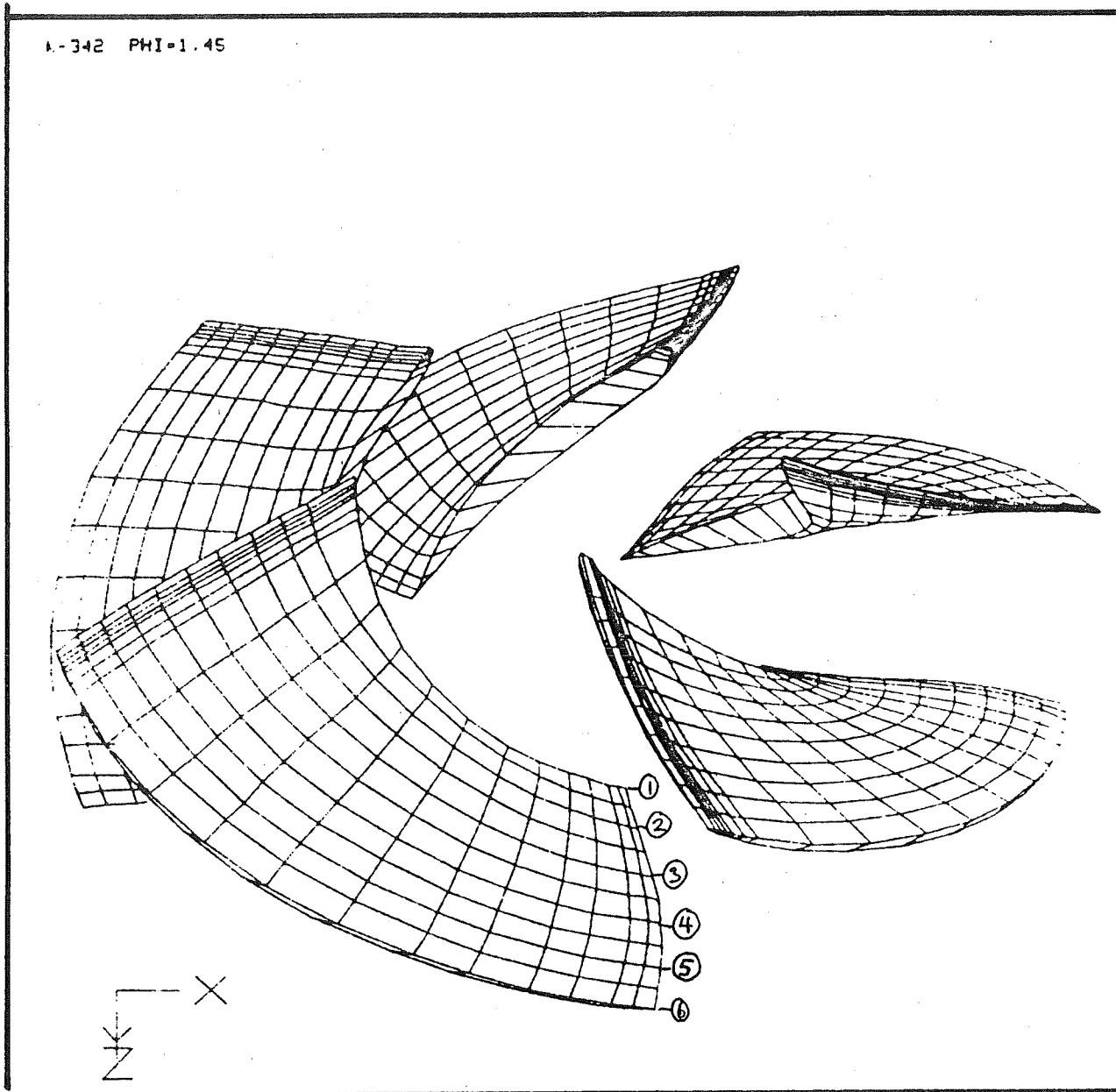


Fig. 15 3-D View of Kaplan Blades

CARACTERISTIQUES DU MODEL

ORDE • 1.00
NOMBRE DE POINT • 10
XTRADOS • 0.0
NTRADOS • 0.0

ACTEUR CONC. • 0.10

ANGLE ROTATION • 0.0
0.3433935 -0.3433935

INTERPOLATION LINEAIRE

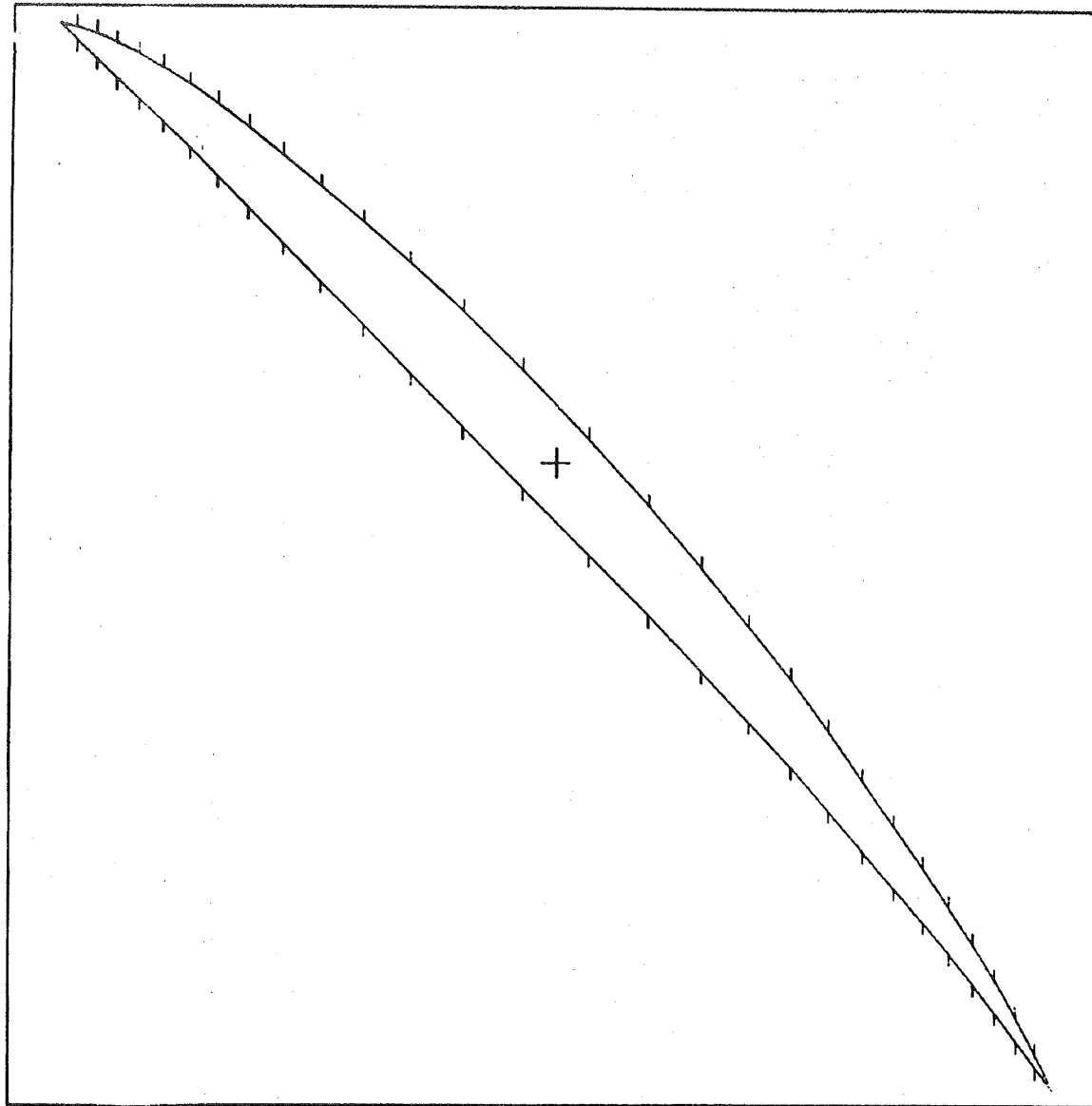


Fig. 16 Developed Profile of Section 2

CHARACTERISTIQUES DU PROFIL

ORDRE = 1.00
NOMBRE DE POINT = 30
EXTRADOS = 30
INTRADOS = 30
FACTEUR CONC. = 0.50
ANGLE ROTATION = 0.0
0.2562680 -0.3826444

INTERPOLATION LINEAIRE

INTERPOLATION DU PROFIL

->(FIN)
->(INITIALISATION
->(LIRE)
->(ECRIRE)
->(INTERPOLATION
->(GRAPHISME
->()-ABREVIATION
ENTRER UNE OPTION,...

ECR
Ecrire le nom du fichier
à écrire.

SECS.PRO
INTERPOLATION DU PROFIL

->(FIN)
->(INITIALISATION
->(LIRE)
->(ECRIRE)
->(INTERPOLATION
->(GRAPHISME
->()-ABREVIATION
ENTRER UNE OPTION,...

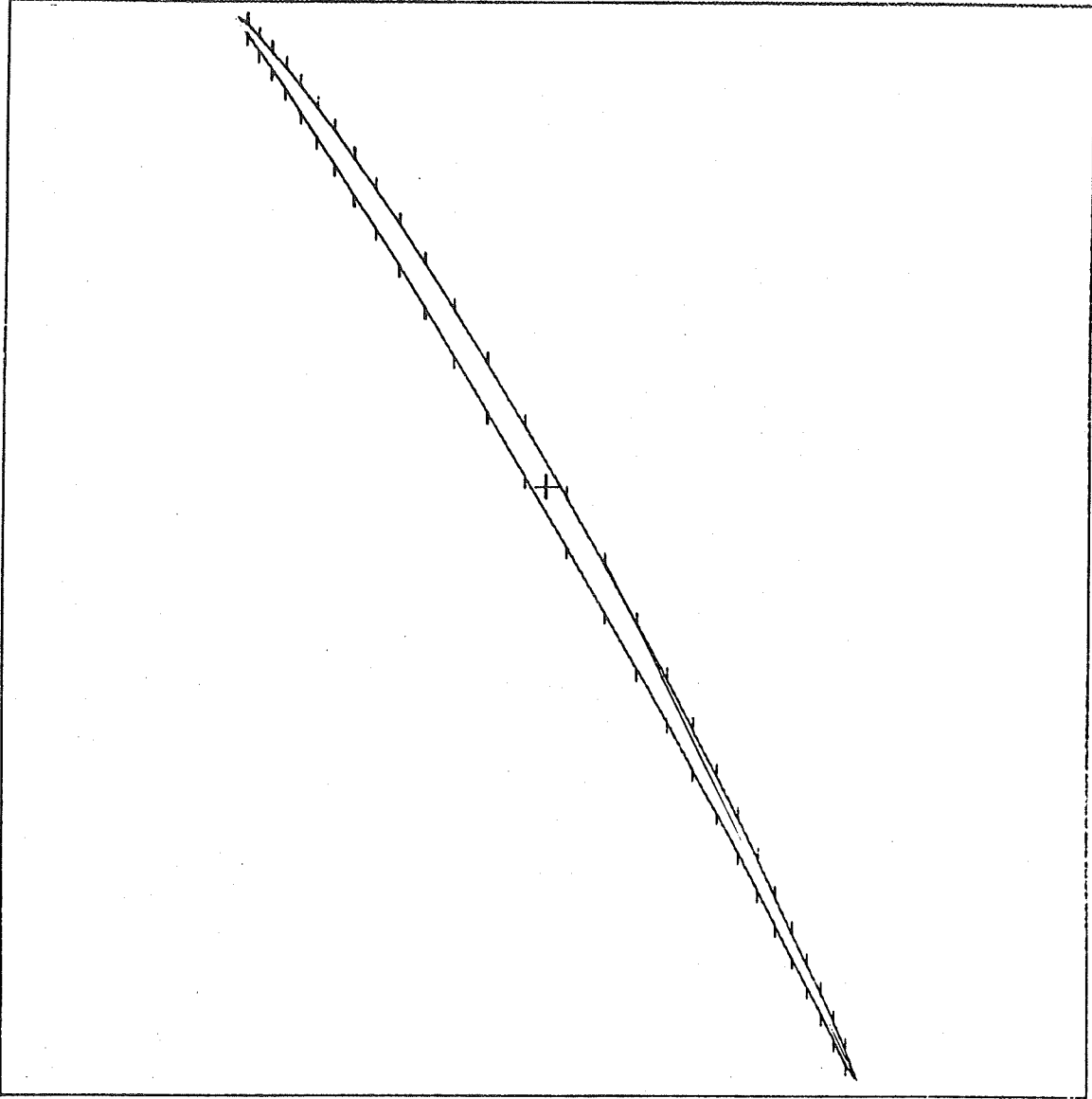


Fig. 17 Developed Profile of Section 5

ANALYSE N349-SEC2

SOLUTION SEC2.RES

ECOLEMENT 'ISOUEUX
REYNOLDS = 10000.

ANGLE PROFIL = -47.00
ANGLE ATTAQUE = -32.93
ANGLE FUITE = -51.68

COEF. CD = 0.1135
COEF. CL = 1.132
COEF. CA = 0.8461
COEF. CT = 0.7612
TORQUE CM = -0.6707

CHARACTERISTIQUES DU PROFIL

PROFIL = SEC2.PRO
ORDRE = 1.000
NOMBRE DE PTS = 30

CHARACTERISTIQUES DE LA CASCADE

CASCADE = SEC2.CAS
NOMBRE DE RANGEES = 27
NO. TOTAL COLONNE = 90
NO. COL. ENTREE = 25
NO. COL. SORTIE = 35

LONG. INTERAUBE = 0.8000
LONG. ENTREE = 0.8000
LONG. SORTIE = 1.200

ANGLE ENTREE (DEG) = -33.00
ANGLE PROFIL (DEG) = -47.00
ANGLE SORTIE (DEG) = -47.00

LONG. RANGEES = 0.6000
LONG. COL. ENTREE = 0.3000
LONG. COL. SORTIE = 0.3000

COMPONENT UX MAX = 1.222
RANG = 4 , COL. = 29)
COMPONENT UX MIN = 0.4827
RANG = 2 , COL. = 54)

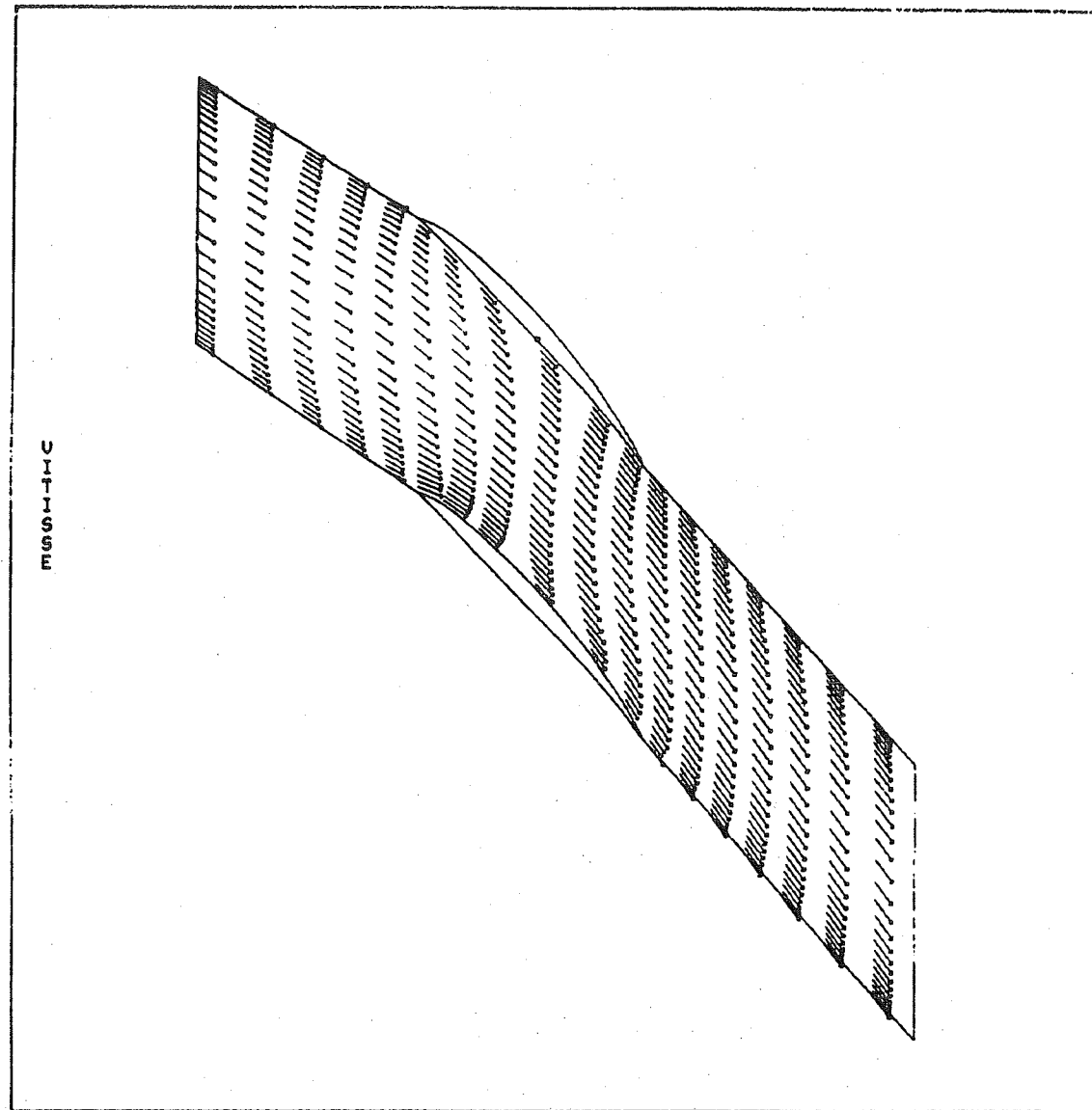


Fig. 18 Velocity Field in Section 2

ANALYSE K349-SEC5

SOLUTION SEC5.REM

COULEMENT VISQUEUX
EYNOLDS = 10000.

ANGLE PROFIL = -60.00
ANGLE ATTAQUE = -57.34
ANGLE FUITE = -61.86

DEF. CD = 0.5536E-01
DEF. CL = 0.4787
DEF. CA = 0.4410
DEF. CT = 0.1841
ORQUE CM = -0.9366

CARACTERISTIQUES DU PROFIL

PROFIL = SEC4.PRO
ORDE = 1.000
NOMBRE DE PTS = 30

CARACTERISTIQUES DE LA CASCADE

CASCADE = SEC5.CAH
NOMBRE DE RANGEES = 27
O. TOTAL COLONNE = 90
O. COL. ENTREE = 25
O. COL. SORTIE = 35

ONG. INTERAUBE = 1.138
ONG. ENTREE = 0.8000
ONG. SORTIE = 1.200

ANGLE ENTREE (DEG) = -57.50
ANGLE PROFIL (DEG) = -60.00
ANGLE SORTIE (DEG) = -60.00

ONG. RANGEES = 0.6000
ONG. COL. ENTREE = 0.3000
ONG. COL. SORTIE = 0.3000

COMPONENT UX MAX = 0.7603
RANG = 2 , COL. = 30)
COMPONENT UX MIN = 0.2645
RANG = 2 , COL. = 54)

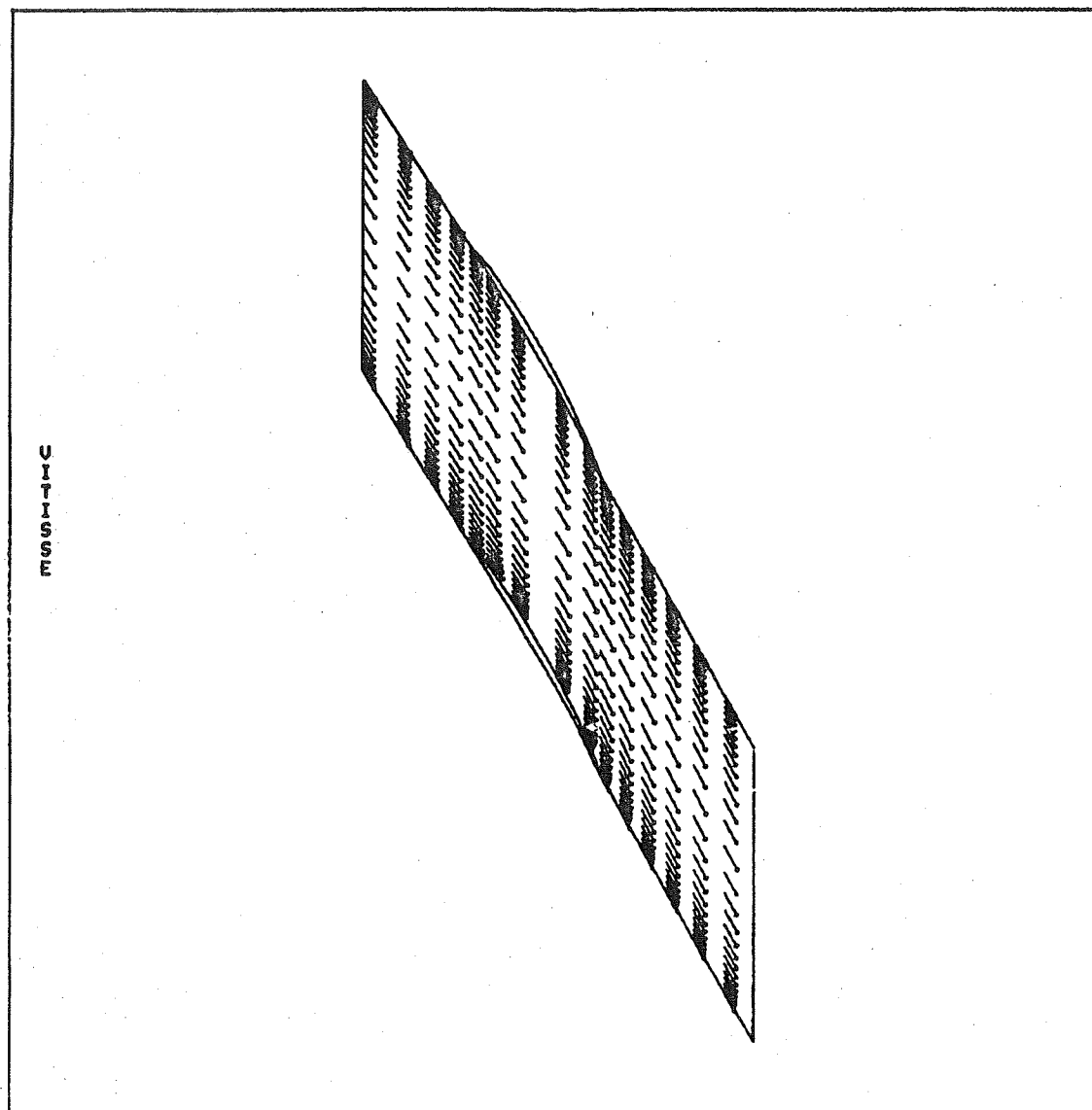


Fig. 19 Velocity Field in Section 5

ANALYSE K349-SEC2

SOLUTION SEC2.RES

COULEMENT VISQUEUX
REYNOLDS = 10000.

ANGLE PROFIL = -47.00
ANGLE ATTAQUE = -32.93
ANGLE FUITE = -51.68

DEF. CD = 0.1135
DEF. CL = 1.132
DEF. CA = 0.8461
DEF. CT = 0.7612
MOQUE CM = -0.6707

CARACTERISTIQUES DU PROFIL

PROFIL = SEC2.PRO
ORDRE = 1.000
NOMBRE DE PTS = 30

CARACTERISTIQUES DE LA CASCADE

CASCADE = SEC2.CAS
NOMBRE DE RANGEES = 27
J. TOTAL COLONNE = 90
J. COL. ENTREE = 25
J. COL. SORTIE = 35

ANG. INTERAUBE = 0.8000
ANG. ENTREE = 0.8000
ANG. SORTIE = 1.2000

ANGLE ENTREE (DEG) = -33.00
ANGLE PROFIL (DEG) = -47.00
ANGLE SORTIE (DEG) = -47.00

INC. RANGEES = 0.6000
INC. COL. ENTREE = 0.3000
INC. COL. SORTIE = 0.3000

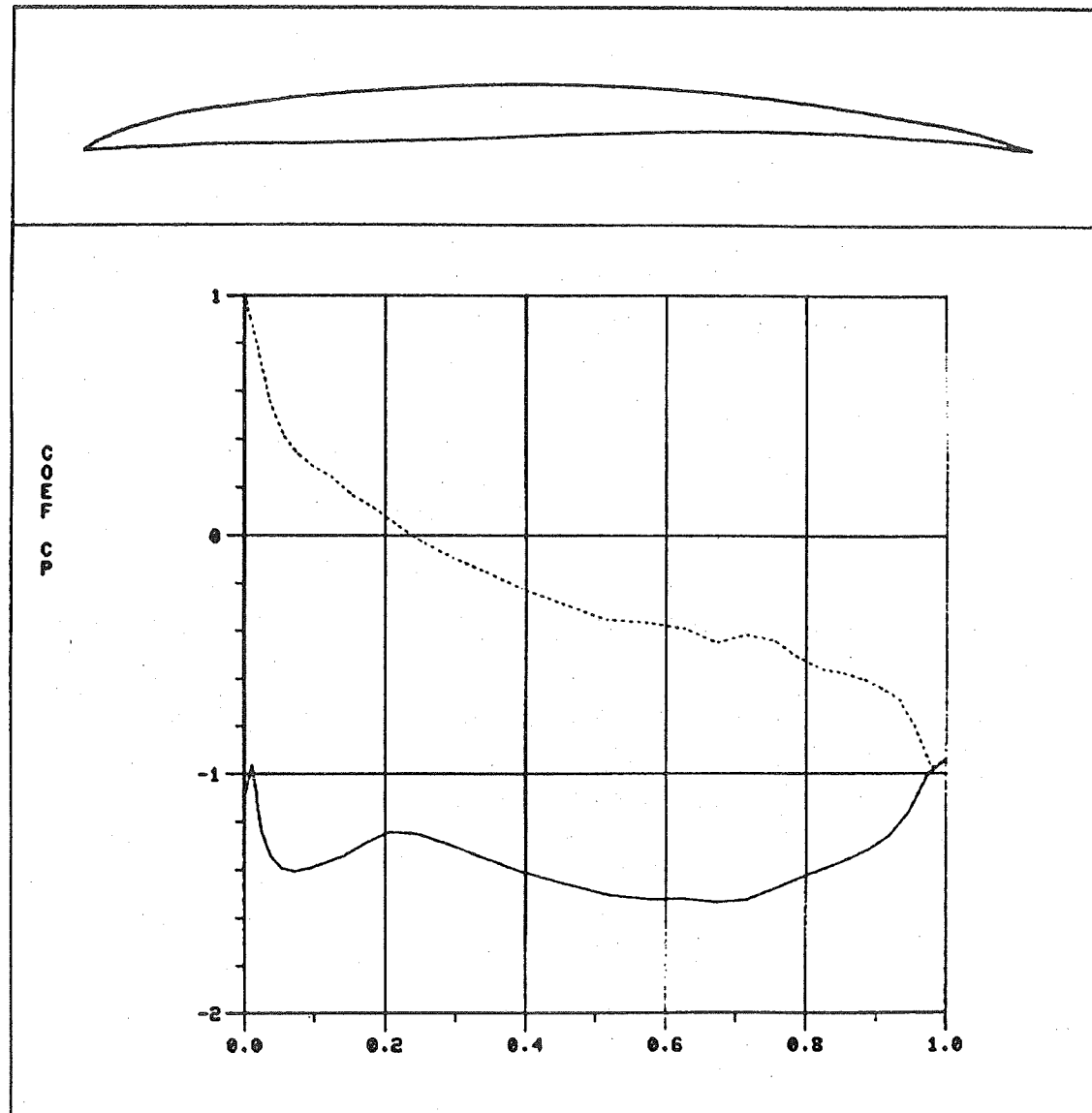


Fig. 20 Pressure Coefficient on Section 5

ANALYSE K349-SECS

OLUTION SECS.REH

COULEMENT VISQUEUX
EYNOLDS = 10000

ANGLE PROFIL = -60.00
ANGLE ATTAQUE = -57.34
ANGLE FUITE = -61.98

DEF. CD = 0.5536E-01
DEF. CL = 0.4787
DEF. CA = 0.4410
DEF. CT = 0.1941
MOMENT CM = -0.9366

CARACTERISTIQUES DU PROFIL

PROFIL = SEC4.PRO
ORDRE = 1.000
OMBRE DE PTS = 30

CARACTERISTIQUES DE LA CASCADE

CASCADE = SECS.CAH
OMBRE DE RANGEES = 27
O. TOTAL COLONNE = 90
O. COL. ENTREE = 25
O. COL. SORTIE = 35

ONG. INTERAUBE = 1.138
ONG. ENTREE = 0.8000
ONG. SORTIE = 1.200

ANGLE ENTREE (DEG) = -57.50
ANGLE PROFIL (DEG) = -60.00
ANGLE SORTIE (DEG) = -60.00

ONG. RANGEES = 0.6000
ONG. COL. ENTREE = 0.3000
ONG. COL. SORTIE = 0.3000

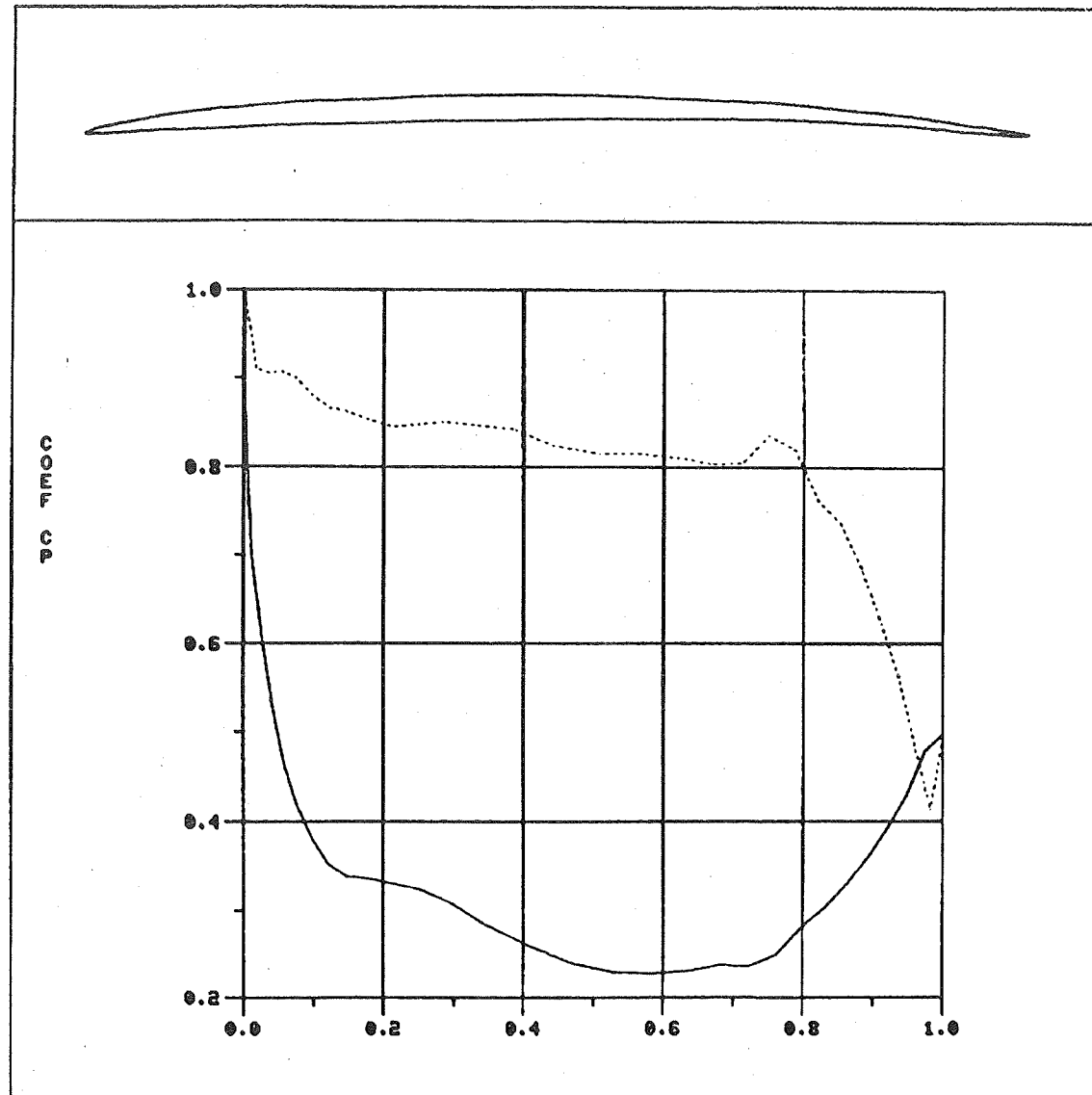


Fig. 21 Pressure Coefficient on Section 2

K-349-4MØ
7886TR

PITOT MEASUREMENT

14-OCT-83

WG= 44.000
PHI= 1.660

PC=ABSOLUTE ◁
PCM=MERIDIAN ◻
-PCX=RADIAL *
-PCY=PERIPHE O
PCZ=AXIAL ◇

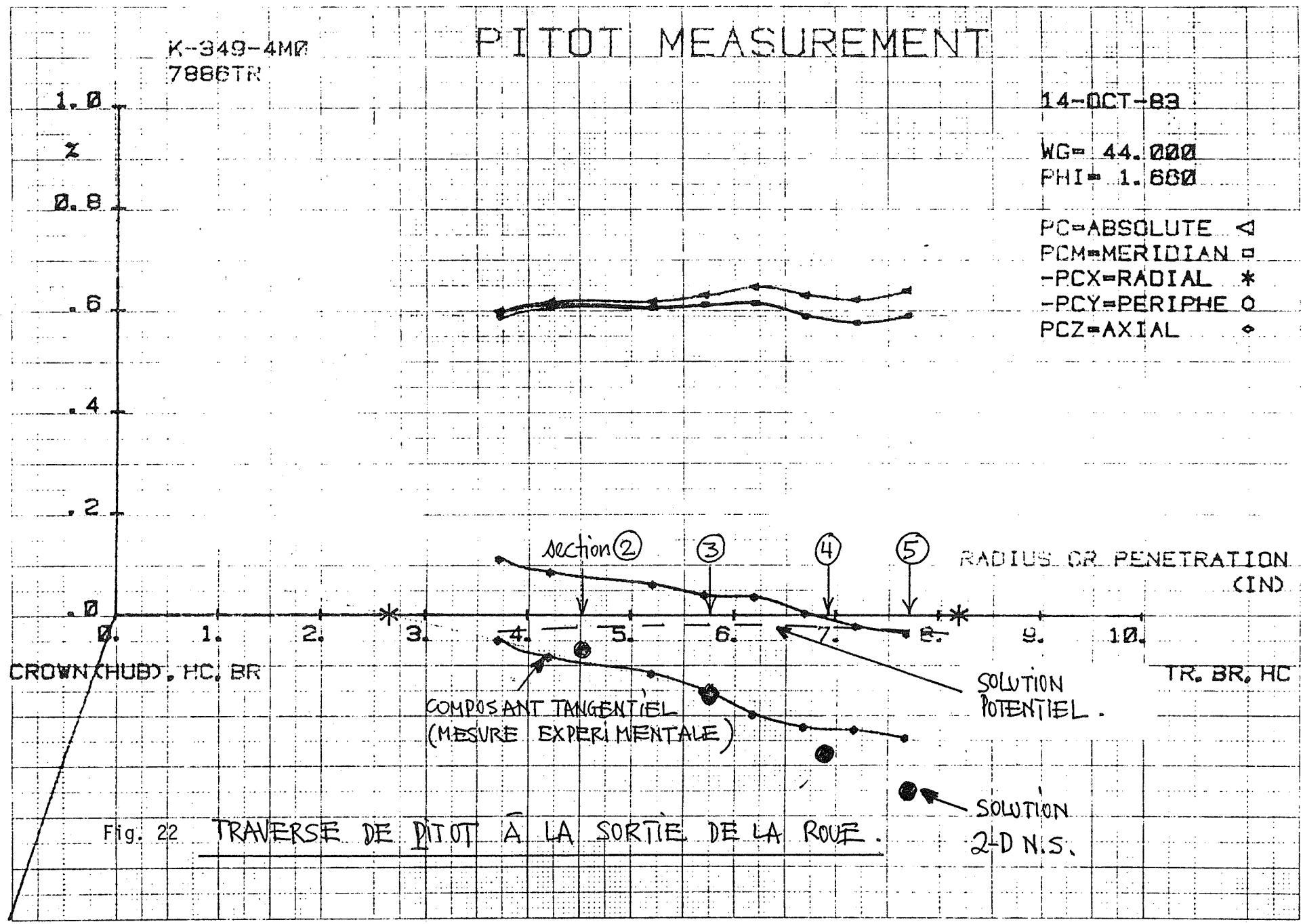


Fig. 22 TRAVERSE DE PITOT A LA SORTIE DE LA ROUE.

ÉCOLE POLYTECHNIQUE DE MONTRÉAL



3 9334 00289357 4